CALIFORNIA INSTITUTE OF TECHNOLOGY

EARTHQUAKE ENGINEERING RESEARCH LABORATORY

SIMULATED EARTHQUAKE MOTIONS

by

P. C. Jennings, G. W. Housner and N. C. Tsai

A report on research conducted under a grant from the National Science Foundation

Pasadena, California

April 1968

SIMULATED EARTHQUAKE MOTIONS

ABSTRACT

Simulated earthquake motions suitable for design calculations are generated with the aid of a digital computer. The artificial accelerograms are sections of a random process with a prescribed power spectral density, multiplied by envelope functions chosen to model the changing intensity at the beginning and end of real accelerograms.

Two each of four different types of accelerograms have been generated to represent ground acceleration for a variety of earthquakes. Type A models the acceleration in a Magnitude 8 shock and type B the motion expected in a Magnitude 7 earthquake. The shaking expected in the epicentral area of a Magnitude 5 or 6 earthquake is modeled by type C and the motion close to the fault in a shallow Magnitude 4 or 5 shock is represented by type D.

The two records of each type were generated to serve as the two horizontal components of earthquake shaking, or as two independent samples of possible ground shaking in the same type of event. Included in the report are accelerograms and derived velocity and displacement curves as well as response spectra.

SIMULATED EARTHQUAKE MOTIONS

by

P. C. Jennings, G. W. Housner and N. C. Tsai

INTRODUCTION

In the earthquake design of important structures it is not uncommon for a digital computer analysis to be made of the response of the structure to a prescribed base acceleration. Recorded earthquake accelerograms are often used for this purpose even though these might not have completely suitable properties. For example, the El Centro, 1940, accelerogram has been used all over the world even though its special character is not really applicable. Because of the rarity of strong earthquakes, the localized extent of the really strong ground shaking, and the seeming proclivity of earthquakes to occur in uninstrumented areas, there are wide gaps in the present-day collection of strong-motion accelerograms. The most significant gap is that the shaking in the vicinity of the causative fault in a truly great (Richter Magnitude 8) earthquake has never been recorded. Also, only three recordings in the epicentral areas of Magnitude 7 earthquakes have been made in the United States (El Centro, California, 1940, Olympia, Washington, 1949 and Taft, California 1952). The statistical fluctuations in intensity, duration and frequency content in these records and records of comparable earthquakes from Mexico and South America indicate that a much larger sample of strong earthquake motion is needed to define adequately the characteristics of strong ground shaking. This is also true of damaging, or potentially damaging shocks of lesser Magnitudes (Richter Magnitude 4 or greater).

Because it will be many years before collections of records of different types will have been assembled, research workers have generated ensembles of simulated earthquakes by various means to help fill the gaps in recorded data. The models for these simulated motions are deduced from examination of the statistical properties of recorded accelerograms, the most significant of which are the duration, intensity and frequency content of the motion. The intensity and frequency content are, in general, functions of time.

Mathematical models of varying complexity have been used or suggested to model accelerograms. These models include a white noise (Housner, 1947, Rosenblueth and others, 1956, 1962, Bycroft, 1960) stationary Gaussian Processes (Tajimi, 1960, Housner and Jennings, 1964, Barstein, 1960), and nonstationary processes of various types (Bolotin, 1960, Bogdanoff et al., 1961, Cornell, 1964, Amin and Ang, 1966, Shinozuka and Sato, 1967).

All of the proposed types of statistical models embody some of the important properties of strong ground motion and the choice of the model to be used depends on the characteristics that are important to the problem at hand. Thus, many of the characteristics of the response of linear, damped structures to earthquake motions can be modeled by the response to white noise (Bycroft 1960) but the frequency content of this model is known to be inaccurate. Housner and Jennings (1964) showed that the key central portion of the acceleration from strong earthquakes could be modeled by sections of a stationary Gaussian process with a spectral density derived from average undamped velocity spectra. Although satisfactory for most response studies, the artificial

earthquakes generated by this process are not appropriate for modeling smaller earthquake motions or for use in studies where the less intense but longer tails of the accelerograms are thought to be significant. An important example is in studies of the tendency of certain soils to liquify under cyclic straining (Seed and Wilson).

To model the shaking in smaller earthquakes (Richter Magnitude of 5 or 6) and to model the tail of larger shocks it is necessary to employ a nonstationary random process. One of the simplest types of nonstationary processes consists of a stationary process multiplied by a time dependent envelope function (Bendat and Piersol, 1966). Amin and Ang (1966) have shown that a filtered Poisson process modified by such an envelope is a satisfactory model for motions expected during large earthquakes. To model the rapid build-up of motion, the central portion of strong shaking, and the decaying tail, Amin and Ang use an envelope function divided into three parts: a) a rapid quadratic build-up in intensity from zero; b) a constant central portion; and c) an exponentially decaying tail.

In the work reported here, the nonstationarity of the accelerogram also is introduced by envelope functions of this general type, but the envelope functions are applied to sections of the same Gaussian random process used previously to model the central portion of strong earthquakes (Housner and Jennings, 1964). The present work also differs from previous efforts in that attention is focused on the preparation of simulated earthquake motions appropriate for use in design calculations of special structures. For this purpose, two each of four different types of accelerograms have been generated to represent ground acccleration

in a variety of earthquakes ranging from a great earthquake, such as occurred in Chile in 1960 or Alaska in 1964, to a small, close shock such as recorded in Parkfield, California in 1966. The accelerograms have been processed, filtered, and scaled to have the properties appropriate to the ground motion they model.

The two accelerograms of each type are intended to serve as two components of the same shock for calculations of two-dimensional motion, or as two independent samples of possible ground shaking in the same type of event. The presentation in this report includes the accelerograms and derived velocity and displacement curves as well as response spectra. Card decks, giving the acceleration ordinates at 1/40 second intervals, will be furnished on request to persons interested in making calculations using these simulated motions.

GENERATION OF EARTHQUAKE MOTION

Summary

The simulation process used can be summarized as follows: A sequence of uncorrelated numbers, normally distributed with mean zero and variance unity is considered to be a collection of sample points of a white noise of a certain duration, sampled at an interval at least twice as short as the smallest period of interest in the final process. This approximation to a white noise is then passed through a second order filter whose properties are chosen to impart to the process the desired frequency content, as measured by the power spectral density.

By multiplying the resulting sections of a stationary Gaussian process by a suitably chosen envelope, the desired nonstationary properties are given to the record. In a manner identical to that used

in processing real earthquakes, (Berg and Housner, 1961) the baseline of the accelerogram is relocated by performing a least squares fit to the velocity of a parabolic correction to the baseline. This correction has the effect of filtering out long period components in the motion (with very small accelerations) which would otherwise impart unrealistic characteristics to the computed ground velocity and displacement. In real accelerograms these long period components are thought to arise from recording and digitizing errors; in the statistical model they are present because of the frequency content of the underlying process.

The parabolic correction to the baseline introduces an offset of the accelerogram at the beginning. For real accelerograms, this corresponds to the ground acceleration present at the time the accelerograph begins to record effectively. Because the simulated motions are intended to model perfectly recorded accelerograms, the acceleration must start from zero and this is accomplished by the addition of a small linear correction to the first second or half-second of the accelerogram.

The response spectra of the simulated earthquakes then were calculated so that their frequency contents could be examined and compared to that of recorded motions, where possible. Undesirable frequency components were then removed by passing the accelerogram through a second order filter, with a relatively long natural period. As employed, this filter progressively diminishes the frequency content of the record at periods longer than its natural period. Frequency components less than its natural period pass through the filter unaltered.

As the last step in the generating process the accelerograms of the different types were scaled to the intensity of shaking appropriate to the earthquakes with which they are associated. Finally the ground acceleration, velocity and displacement of the scaled motions were plotted and are presented herein along with the response spectra of the finished accelerograms.

Details of the Generation Process

Consider a stationary random process $\{\ddot{x}(t)\}$ which can be taken to be normally distributed with a mean of zero and a variance of unity. $\ddot{x}(t)$ has the units of acceleration. Let $E(t)$ be the envelope function which describes the manner in which the intensity of the desired nonstationary process varies with time. Members of a nonstationary ensemble $\{\ddot{z}_1(t)\}$ then can be defined by

$$\ddot{z}_1(t) = E(t)\,\ddot{x}(t) \tag{1}$$

It follows from the properties of $\{\ddot{x}(t)\}$ that $\{\ddot{z}_1(t)\}$ will be Gaussian with mean zero and variance $E^2(t)$. The duration of the nonstationary process is prescribed by letting $E(t)$ be non-zero only over a fixed time interval.

In general, the frequency characteristics of $\{\ddot{z}_1(t)\}$ will depend both on $E(t)$ and $\{\ddot{x}(t)\}$. However, if $E(t)$ varies slowly with respect to the frequencies of interest, the frequency content of $\{\ddot{z}_1(t)\}$ will be determined primarily by $\{\ddot{x}(t)\}$. This will occur, for example, if $E(t)$ has a constant value over a major fraction of the interval for which it is non-zero.

For this work, $\{\ddot{x}(t)\}$ is the stationary process designed by

Housner and Jennings (1964) to model the strong central portion of the accelerograms recorded during strong earthquakes. In that study it was shown that accelerograms which are portions of this random process produced response spectra and ground velocity and displacement curves which resembled closely corresponding results for real earthquake motions. The frequency content of the process was selected so the average spectra of the real and artificial earthquakes matched closely. The details of the generation of $\{\ddot{x}(t)\}$ are available in the literature (Jennings, 1963, Housner and Jennings, 1964) and will not be repeated here. In essence, the process $\{\ddot{x}(t)\}$ is generated by passing a Gaussian white noise through a second order linear filter (one degree of freedom oscillator) which determines the power spectral density of the resulting output. The spectral density was taken from a relation shown to exist between the power spectral density of $\{\ddot{x}(t)\}$ and the average undamped velocity spectra of four of the strongest earthquake motions so far recorded.

Therefore, the process $\{\ddot{z}_1(t)\}$ already contains many of the characteristics desired for the simulated accelerograms, and the primary purpose of the envelope function $E(t)$ in Equation 1 is to specify further how the intensity of the acceleration varies with time, from an initial build-up of intensity to the final decay to a negligible value.

Four envelope functions $E(t)$ were selected to model four different types of earthquake motion which are thought to be of significance for engineered structures. The four kinds of motion are labeled type A, B, C, and D. The envelope functions for the different types are

shown in Figures 1 through 4. Because of Eq. 1, these plots of E(t) show the relative magnitude of the variance of $\{\ddot{z}_1(t)\}$ as a function of time.

Earthquake Type A is of 120 seconds total duration and is designed to represent an upper bound for the ground motions expected in the vicinity of the causative fault during an earthquake having a Richter Magnitude of 8 or greater. Such motion has not yet been recorded but studies have shown (Housner, 1965) that such motions should have many of the properties exhibited by the type A accelerograms. Type B motion has a duration of 50 seconds and is intended to model the shaking close to the fault in a Magnitude 7 earthquake, such as occurred in El Centro, California in 1940 and in Taft, California in 1952.

The duration of earthquake C is 12 seconds; this type of simulated motion models that expected in the epicentral region of a Magnitude 5.5 to 6 shock, such as occurred in San Francisco in 1957 and in Helena, Montana in 1935. In highly seismic regions such shocks could occur several times in the life of a structure. Earthquake type D, with a duration of 10 seconds, and a much smaller duration of strong shaking, is intended to model the shaking quite close to the fault in a very shallow Magnitude 4.5 to 5.5 earthquake. Such a shock was recorded at several stations in Parkfield, California in 1966; the most remarkable features of the accelerogram recorded 200 ft from the fault were that the maximum acceleration was 50 percent g and the duration of strong motion was 1.5 seconds (Housner and Trifunac, 1967).

In common with most recorded strong motion accelerograms, the process $\{\ddot{z}_1(t)\}$ from Equation 1 does not have a reasonable baseline,

as evidenced by the behavior of the integrated ground velocity $\{\dot{z}_1(t)\}$. Figures 5(a) and 5(b) give $\ddot{z}_1(t)$ and $\dot{z}_1(t)$ for earthquake C-1 and show the ground velocity positive for the later half of the record and trending to a non-zero value at the end of the excitation. Such behavior is not realistic and is eliminated by a small adjustment of the acceleration baseline in the same manner used to adjust the same trend in real accelerograms (Berg and Housner, 1961). The adjusted accelerogram and the derived velocity for earthquake C-1 are shown in Figures 5(c) and (d), which show that the effect of the adjustment on the acceleration is almost indecernible, and that the higher frequency content of the ground velocity is not altered.

The correction to the accelerogram $\ddot{z}_1(t)$ takes the form of a parabolic addition to the baseline. Thus, the modified acceleration $\ddot{z}_2(t)$ is given by

$$\ddot{z}_2(t) = \ddot{z}_1(t) + a_1 + a_2 t + a_3 t^2 \qquad (2)$$

It was found that the magnitude of the coefficients a_i were usually proportional to the duration of the accelerogram. Thus, a_1, the small nonzero start of the accelerogram $\ddot{z}_2(t)$, was larger for types A and B than for the shorter C and D types. The magnitude of a_1 for earthquake C-1 is shown in Figure 5(c). Because accelerograms starting from zero were desired, this feature was removed by a linear correction of one second duration for types A and B and 1/2 second duration for types C and D. As can be judged from Figure 5(c), the effect of a linear correction applied to the first half-second of earthquake C-1 would have a negligible effect on the accelerogram, and

therefore a corresponding negligible effect on the spectra calculated from the acceleration. The effects of this correction on the ground velocity and displacement are not negligible but are overridden by the effects of subsequent filtering.

Designating the acceleration after the least-square modification and the correction at the beginning of the motion as $\ddot{z}_3(t)$, this acceleration was then filtered to give a frequency content, as judged by response spectra and ground velocity and displacement curves, appropriate to the motions which were modeled. The filter used was a second order linear filter which corresponds physically to a one degree of freedom oscillator as shown in Figure 6(a). The input at the base is $-\ddot{z}_3(t)$ and the filtered output is the relative acceleration $\ddot{z}(t)$.

The effect of this filter can be seen by examining the equation of motion:

$$\ddot{z} + 2n_f \omega_f \dot{z} + \omega_f^2 z = \ddot{z}_3(t) \qquad (3)$$

Equation 3 implies that if ω_f is small compared to the component of $\ddot{z}_3(t)$ at a particular frequency, then in this frequency range $\ddot{z}(t) \approx \ddot{z}_3(t)$. Conversely, for excitation with low frequency compared to ω_f, the mass moves with the base and $\ddot{z}(t)$ is much smaller than $\ddot{z}_3(t)$.

The behavior described above can be examined mathematically by comparing the relative steady-state response to sinusoidal excitation at various frequencies, as is done in Figure 6(b). This plot, called the transfer function, is the ratio of the steady-state magnitudes of $\ddot{z}(t)$ and $\ddot{z}_3(t)$, for the special case in which the excitation is

$$z_3(t) = A \sin \omega t \qquad (4)$$

therefore a corresponding negligible effect on the spectra calculated from the acceleration. The effects of this correction on the ground velocity and displacement are not negligible but are overridden by the effects of subsequent filtering.

Designating the acceleration after the least-square modification and the correction at the beginning of the motion as $\ddot{z}_3(t)$, this acceleration was then filtered to give a frequency content, as judged by response spectra and ground velocity and displacement curves, appropriate to the motions which were modeled. The filter used was a second order linear filter which corresponds physically to a one degree of freedom oscillator as shown in Figure 6(a). The input at the base is $-\ddot{z}_3(t)$ and the filtered output is the relative acceleration $\ddot{z}(t)$.

The effect of this filter can be seen by examining the equation of motion:

$$\ddot{z} + 2n_f \omega_f \dot{z} + \omega_f^2 z = \ddot{z}_3(t) \tag{3}$$

Equation 3 implies that if ω_f is small compared to the component of $\ddot{z}_3(t)$ at a particular frequency, then in this frequency range $\ddot{z}(t) \approx \ddot{z}_3(t)$. Conversely, for excitation with low frequency compared to ω_f, the mass moves with the base and $\ddot{z}(t)$ is much smaller than $\ddot{z}_3(t)$.

The behavior described above can be examined mathematically by comparing the relative steady-state response to sinusoidal excitation at various frequencies, as is done in Figure 6(b). This plot, called the transfer function, is the ratio of the steady-state magnitudes of $\ddot{z}(t)$ and $\ddot{z}_3(t)$, for the special case in which the excitation is

$$z_3(t) = A \sin \omega t \tag{4}$$

the transfer function is found to be

$$T_r\left(\frac{\omega}{\omega_f},\ n_f\right) = \frac{\left(\frac{\omega}{\omega_f}\right)^2}{\sqrt{\left[1 - \left(\frac{\omega}{\omega_f}\right)^2\right]^2 + \left[2n_f \frac{\omega}{\omega_f}\right]^2}} \tag{5}$$

To avoid an undesirable resonance for frequency components near ω_f, the damping of the filter must be rather large and it is easily shown that particularly good performance is achieved if $n_f = 1/\sqrt{2}$. Substituting in Equation 5 and expressing the results in terms of the period yields

$$T_r\left(\frac{T}{T_f}\right) = \frac{1}{\sqrt{1 + \left(\frac{T}{T_f}\right)^4}} \tag{6}$$

This is the function plotted in Figure 6(b). From Equation 6 and Figure 6(b) it is seen that the filter passes essentially unmodified periodic components less than T_f, whereas components exceeding T_f are greatly diminished so that it functions as a low-pass filter.

The diminution of the longer period components of the simulated earthquake motions can be seen from a comparison of the spectra of $\ddot{z}_2(t)$ in Figure 7(a) and of $\ddot{z}(t)$ in Figure 7(b). Again this illustrative example is for earthquake C-1. In this case the natural period of the filter used was two seconds, and the rapid decrease in the spectra of the filtered motion for periods greater than two seconds shows up clearly. Also Figure 7 shows that the effect of the filter decreases rapidly for periods progressively shorter than two seconds.

The values of T_f used for the different types of simulated earthquakes were chosen primarily on the basis of the response spectra

of the filtered motion for the shorter earthquakes and on the basis of the frequency content of the ground velocity and displacement for the larger earthquakes. On these bases, the values of T_f were chosen to be two seconds for earthquake types C and D and seven seconds for earthquake types A and B. Real earthquakes of 120 or 50 seconds duration may well have period components larger than about seven seconds, but the acceleration associated with the frequency of motion appears to be so low that it cannot be recorded accurately by existing strong-motion accelerographs. Therefore, it was judged appropriate that they be dimished greatly. The choice of seven seconds as the filter frequency is, of course, somewhat arbitrary, but gave acceptable results. For response spectra calculated for periods up to four seconds, this filtering has no appreciable effect.

It is noteworthy that the response spectra for the shorter simulated earthquakes tend to come together for large values of T, for example in Figure 7 (b). This effect also has been observed for spectra of real earthquakes of this duration and illustrates the well-known fact that for large periods the maximum value of the displacement of the simple oscillator used to calculate spectra must eventually approach the maximum value of the ground displacement.

Such behavior is illustrated in Figure 8 which shows the time history of response of an oscillator with a natural period of four seconds to earthquake D-1 (Figure 15). The undamped response is given in Figure 8 (a), the 10 percent damped response in Figure 8 (b), and the displacement of the ground (with a change of sign) calculated from

acceleration D-1 is shown in Figure 8 (c). The curves in Figure show that the displacement of the oscillator follows closely the ground displacement in this period range.

Scaling

To complete the generation of the simulated earthquakes, they must be scaled to intensities representative of the earthquakes they are intended to model; heretofore in the generation process the scale of the accelerograms has been arbitrary. For earthquake types A, B, and C, the basis of the scaling was the average of the 20 percent damped spectrum intensity of the two records of each type. For earthquake type D, the maximum acceleration was used.

The 20 percent damped spectrum intensity is defined as (Housner, 1952)

$$SI_{0.20} = \int_{0.1}^{2.5} S_v(0.20,\ T)\, dT \qquad (7)$$

in which S_v is the velocity spectra as a function of period T. In this report the integral of Equation 7 was evaluated using ωS_d rather than S_v; this substitution is not expected to be significant over the period range involved in Eq. 7 (Hudson, 1962).

The accelerograms of earthquake type A were scaled so that the average value of the spectrum intensity is 150 percent as strong as the average spectrum intensity of the two components of the El Centro, 1940 record. Earthquake type B was scaled so the average spectrum intensity would equal the average spectrum intensity of the El Centro, 1940 record. The average intensity of the two earthquakes of type C was set equal to the average of the two components recorded

at Golden Gate Park, San Francisco, during the 1957 earthquake. The scale factor needed to produce the required intensities for the simulated motion is just the ratio of spectrum intensity of the appropriate real earthquake to the spectrum intensity of the simulated motion as generated.

Earthquake type D is intended to model the motion recorded very close to the causative fault in a small earthquake. For this motion the spectrum intensity does not measure well the scale of the motion and the maximum acceleration was used instead. For both motions of type D, the maximum acceleration was scaled to be 0.50g, the maximum acceleration recorded in the Parkfield shock (Cloud and Perez, 1967).

Table I summarizes the primary characteristics of the various types of simulated earthquake motions and includes the duration of the strong portion of the envelope function E(t); the period of the system used to filter the motion; the spectral intensities of the unscaled motion; and the scale factors needed to bring the motion up to the desired intensity. The absolute values of the scale factors have little meaning, but the relative values needed to produce the desired motions give some insight into the scaling process.

Some idea of the statistical fluctuations in the simulated motions can be found also from Table I. The variation of the spectrum intensity between two motions of the same type is about the same as has been observed between two horizontal components of the same earthquake motion.

The accelerograms can, of course, be scaled as desired to represent various intensities of shaking, and by a change of time-scale can be made to represent ground motions with different frequency content. For example, by a 2 to 1 change of time-scale, earthquake A-1 can represent 60 seconds of higher frequency ground motion with 40 percent g maximum acceleration similar to the accelerogram recorded in Lima, Peru, 17 October 1966.

PRESENTATION OF RESULTS

The earthquake accelerograms in their final form are presented together with the velocity and displacement curves in Figures 9 through 16 wherein it should be noted that the time scales are different for the different types of motion.

Response spectra for the simulated motions are given in Figures 17 through 24. The spectra given are ωS_d plotted as a function of period. These spectra have nearly all the properties of the velocity spectra and have been called the "Pseudo-velocity spectra." Their advantage over the velocity spectra lies in the fact that division of the spectrum value by ω produces the exact value of the maximum displacement, and multiplication by ω produces the exact value of the maximum shear force per unit mass. Similar operations on the velocity spectra are only approximately true and are not always satisfactory.

Because of their convenience in design, the ωS_d spectra are plotted also on tripartite logarithmic paper in Figures 25 through 32. This method of presentation allows the maximum displacement and maximum acceleration to be read directly from the inclined axes.

SUMMARY AND CONCLUSIONS

The simulated earthquake motions presented in Figures 9 through 16, with spectra shown in subsequent figures, are intended to model four types of strong earthquake motions and have been shaped and scaled accordingly. The two motions of each kind can be used to model the two horizontal components of the same shock, or can be used to represent a repetition of the same type of earthquake.

Type A is intended to model the shaking in the vicinity of the fault in a great (Richter Magnitude 8 or greater) earthquake, and has a spectrum intensity half again as strong as that for the El Centro, 1940 shock. Earthquakes of Type B are designed to represent the strong shaking in a Magnitude 7 or greater earthquake, and have the same spectrum intensity as the El Centro, 1940 record.

The earthquakes of Type C model the shaking expected in the epicentral region of a Magnitude 5.5 to 6 earthquake, and have the same average intensity as the record obtained at Golden Gate Park during the 1957 San Francisco earthquake. For earthquakes of Type D, which model the shaking close to the fault in a shallow Magnitude 4.5 to 5.5 earthquake, the motions have been scaled to have a maximum acceleration of 50 percent g, the maximum acceleration recorded in the Parkfield, California earthquake of 1966.

It is concluded that the simulated earthquakes are reasonably representative of the type of motions modeled and from the generation process it is concluded that most of the characteristics of strong ground motion records obtained on firm ground can be modeled by simple random processes and the statistical fluctuations which are inherent

in such processes.

The artificial earthquakes were generated to augment the number of accelerograms available for use in digital response studies of structures, and copies or listings of the acceleration decks, consisting of acceleration ordinates at 1/40 second intervals, will be made available upon request.

ACKNOWLEDGMENT

Appreciation is extended to the National Science Foundation for partial support of this research under NSF Grant 1197X.

TABLE I

SUMMARY OF PROPERTIES OF SIMULATED EARTHQUAKES

(1)	(2)	(3)	(4)	(5)	(6)
Simulated Earthquake Type	Total Duration (sec)	Duration of the Strong Motion Portion with Constant Envelope (sec)	Filter Period T_f (sec)	Unscaled Damped Spectrum Intensity	Scale Factor to Produce Final Motion
A	120	29	7	0.409 (A-1) 0.420 (A-2)	9.21
B	50	11	7	0.330 (B-1) 0.244 (B-2)	9.44
C	12	2	2	0.354 (C-1) 0.271 (C-2)	1.56
D	10	0.5	2		20 (D-1) 16 (D-2)

REFERENCES

Amin, M., and Ang, A. H.-S., "A Nonstationary Stochastic Model for Strong-Motion Earthquakes," Structural Research Series No. 306, University of Illinois, Department of Civil Engineering, April, 1966.

Barstein, M. F., "Application of Probability Methods for Designing the Effect of Seismic Forces on Engineering Structures," Proceedings of the Second World Conference on Earthquake Engineering, Tolyo and Kyoto, Japan, Vol. II, July, 1960, pp. 1467-1482.

Bendat, J. S. and Piersol, A. G., Measurement and Analysis of Random Data, John Wiley and Sons, New York, 1966.

Berg, G. V. and Housner, G. W., "Integrated Velocity and Displacement of Strong Earthquake Ground Motion," Bulletin of the Seismological Society of America, vol. 51, No. 2, April, 1961, pp. 175-189.

Bogdanoff, J. L., Goldberg, J. E., and Bernard, M. C., "Response of a Simple Structure to a Random Earthquake-like Disturbance," Bulletin of the Seismological Society of America, vol. 51, No. 2, April 1961, pp. 293-310.

Bolotin, V. V., "Statistical Theory of Aseismic Design of Structures," Proceedings of the Second World Conference on Earthquake Engineering, Tokyo and Kyoto, Japan, vol. II, July 1960, pp. 1365-1374.

Bycroft, G. N., "White Noise Representation of Earthquakes," Journal of the Engineering Mechanics Division, ASCE, vol. 86, No. EM2, April 1960, pp. 1-16.

Cloud, W. K., and Perez, P., "Accelerogram - Parkfield Earthquake," Bulletin of the Seismological Society of America, vol. 57, No. 6 December 1967, pp. 1179-1192.

Cornell, C. A., "Stochastic Process Models in Structural Engineering," Technical Report No. 34, Stanford University, Department of Civil Engineering, May, 1964.

Housner, G. W., "Characteristics of Strong-Motion Earthquakes," Bulletin of the Seismological Society of America, vol. 37, No. 1, January, 1947, pp. 19-31.

Housner, G. W., "Spectrum Intensities of Strong Motion Earthquakes," Proceedings of the Symposium of Earthquake and Blast Effects on Structures, Earthquake Engineering Research Institute, 1952.

Housner, G.W., "Intensity of Earthquake Ground Shaking Near the Causative Fault," Proceedings of the Third World Conference on Earthquake Engineering, vol. I, Auckland and Wellington, New Zealand, January, 1965, pp. III-94 to III-115.

Housner, G.W. and Jennings, P.C., "Generation of Artificial Earthquakes," Journal of the Engineering Mechanics Division, ASCE, vol. 90, No. EM1, February 1964, pp. 113-150.

Housner, G. W. and Trifunac, M.D., "Analysis of Accelerograms-Parkfield Earthquake," Bulletin of the Seismological Society of America, vol. 57, No. 6, December, 1967, pp. 1179-1192.

Hudson, D.E., "Some Problems in the Application of Spectrum Techniques to Strong-Motion Earthquake Analysis," Bulletin of the Seismological Society of America, vol. 52, No. 2, April, 1962, pp. 417-430.

Jennings, P.C., "Response of Simple Yielding Structures to Earthquake Excitation," Earthquake Engineering Research Laboratory, California Institute of Technology, Pasadena, 1963.

Rosenblueth, E., "Some Applications of Probability Theory in Aseismic Design," Proceedings of the World Conference on Earthquake Engineering, Berkeley, California, June, 1956, pp. 8-1 to 8-18.

Rosenblueth, E. and Bustamante, J.E., "Distribution of Structural Response to Earthquakes," Journal of the Engineering Mechanics Division, ASCE, vol. 88, No. EM3, June, 1962, pp. 75-106.

Seed, H.B., and Wilson, S.D., "The Turnagain Heights Landslide in Anchorage, Alaska," Department of Civil Engineering, Institute of Transportation and Traffic Engineering, University of California, Berkeley.

Shinozuka, M. and Sato, Y., "Simulation of Nonstationary Random Processes," Journal of the Engineering Mechanics Division, ASCE, vol. 93, No. EM1, February 1967, pp. 11-40.

Tajimi, H., "A Statistical Method of Determining the Maximum Response of a Building Structure During an Earthquake," Proceedings of the Second World Conference on Earthquake Engineering, Tokyo and Kyoto, Japan, vol. II, July, 1960, pp. 781-797.

LIST OF FIGURES

Figure Number (cont'd)	Caption (cont'd)
17	ωS_d spectrum for earthquake A-1
18	ωS_d spectrum for earthquake A-2
19	ωS_d spectrum for earthquake B-1
20	ωS_d spectrum for earthquake B-2
21	ωS_d spectrum for earthquake C-1
22	ωS_d spectrum for earthquake C-2
23	ωS_d spectrum for earthquake D-1
24	ωS_d spectrum for earthquake D-2
25	Tripartite logarithmic plot of spectra for earthquake A-1
26	Tripartite logarithmic plot of spectra for earthquake A-2
27	Tripartite logarithmic plot of spectra for earthquake B-1
28	Tripartite logarithmic plot of spectra for earthquake B-2
29	Tripartite logarithmic plot of spectra for earthquake C-1
30	Tripartite logarithmic plot of spectra for earthquake C-2
31	Tripartite logarithmic plot of spectra for earthquake D-1
32	Tripartite logarithmic plot of spectra for earthquake D-2.

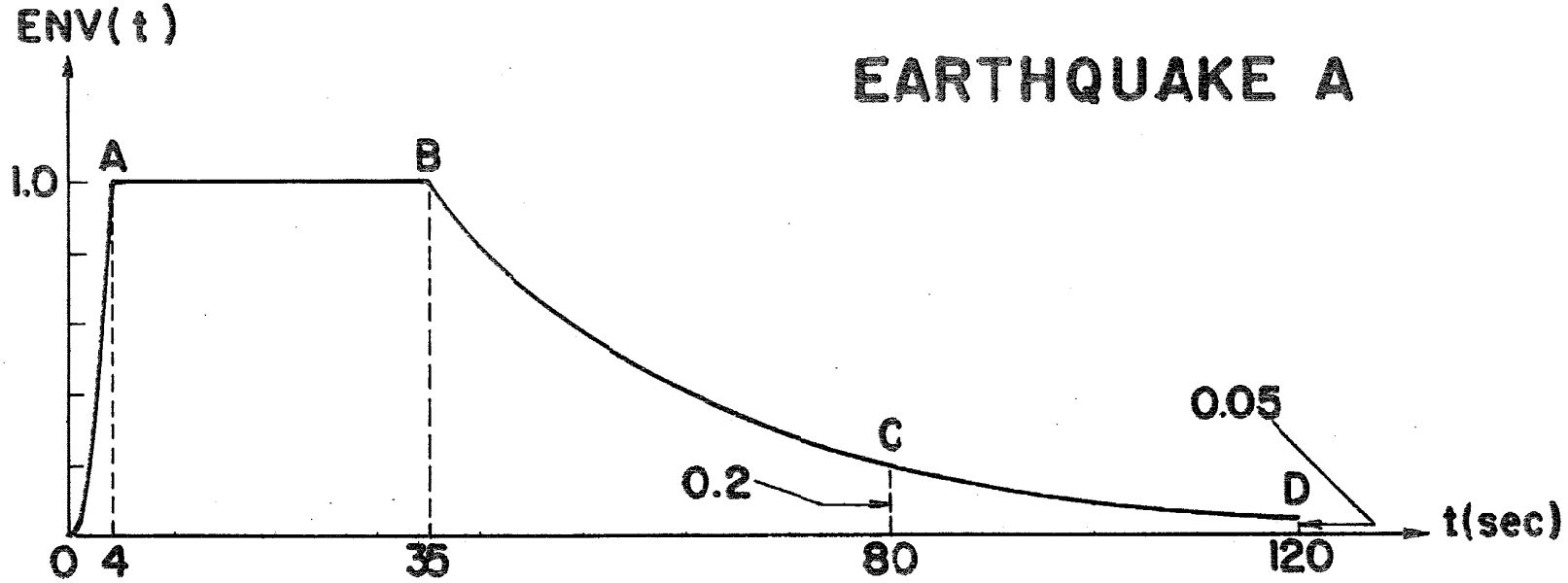

$$OA: \quad ENV(t) = t^2/16$$

$$AB: \quad 1.0$$

$$BC: \quad \exp(-0.0357(t-35))$$

$$CD: \quad 0.05 + 0.0000938(120-t)^2$$

Figure 1

Envelope function for earthquake type A

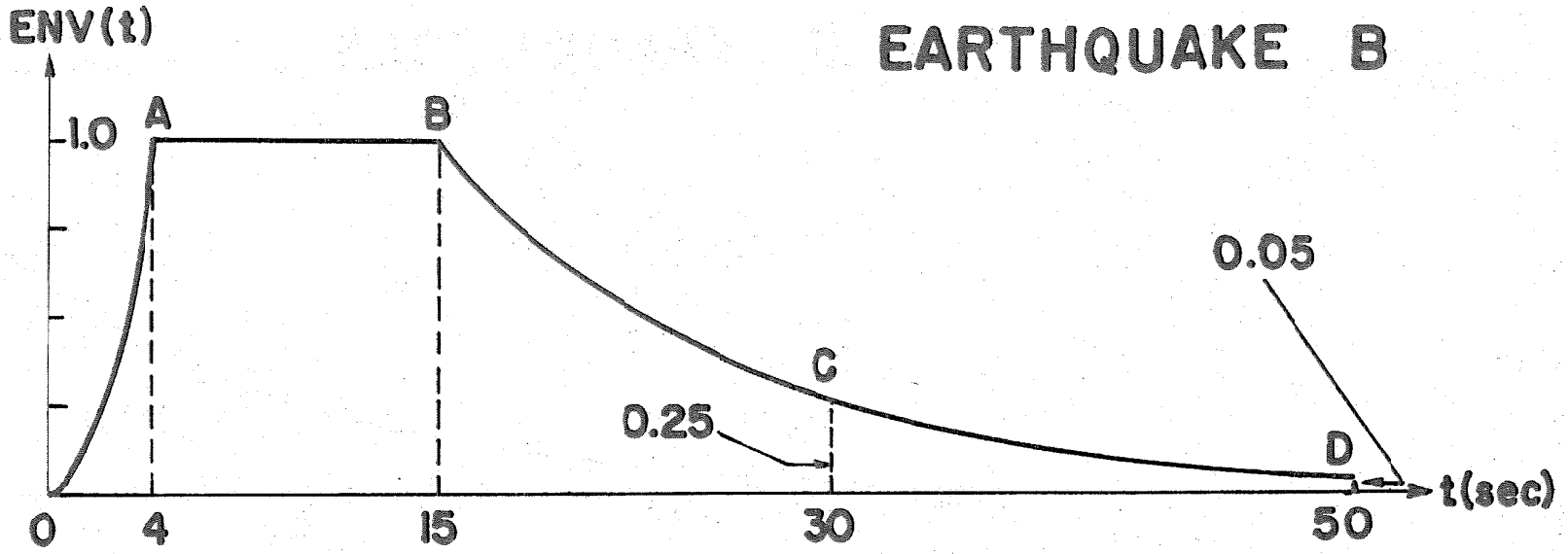

$$OA: \quad ENV(t) = t^{1}/16$$

$$AB: \quad 1.0$$

$$BC: \quad \exp[-0.0992(t-15)]$$

$$CD: \quad 0.05 + 0.005(50-t)^{2}$$

Figure 2

Envelope function for earthquake type B

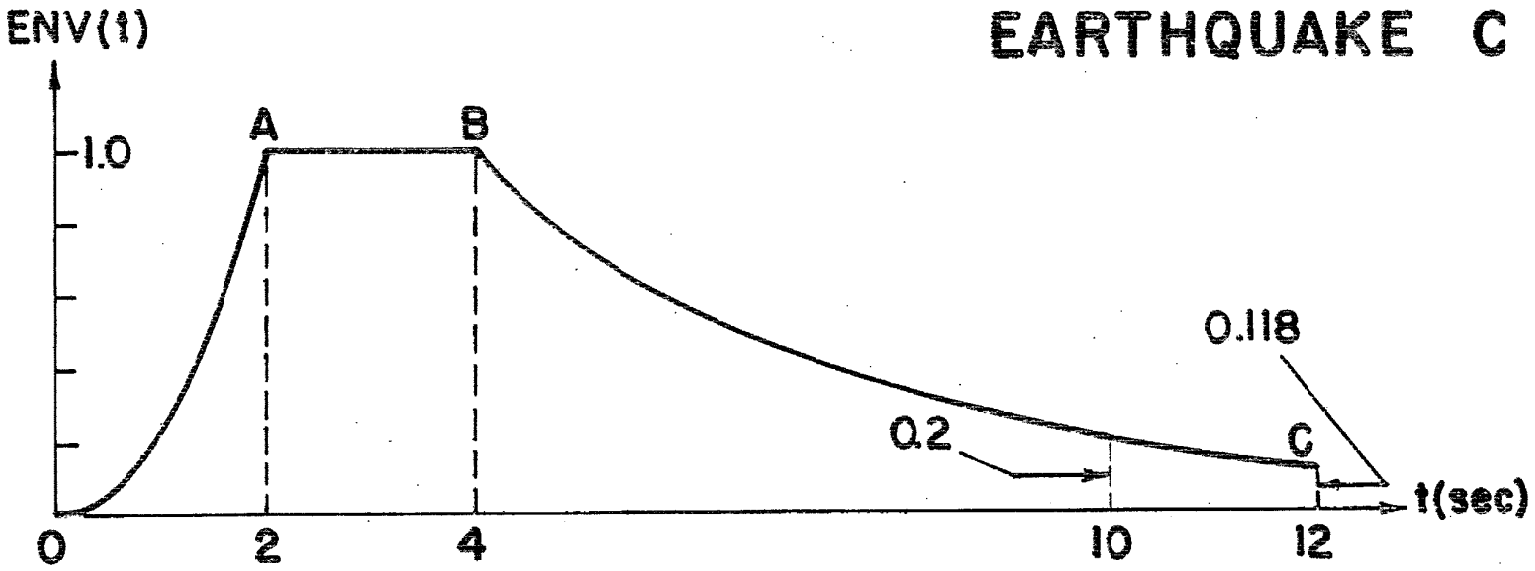

$OA: \quad ENV(t) = t^2/4$

$AB: \quad 1.0$

$BC: \quad \exp[-0.268(t-4)]$

Figure 3

Envelope function for earthquake type C

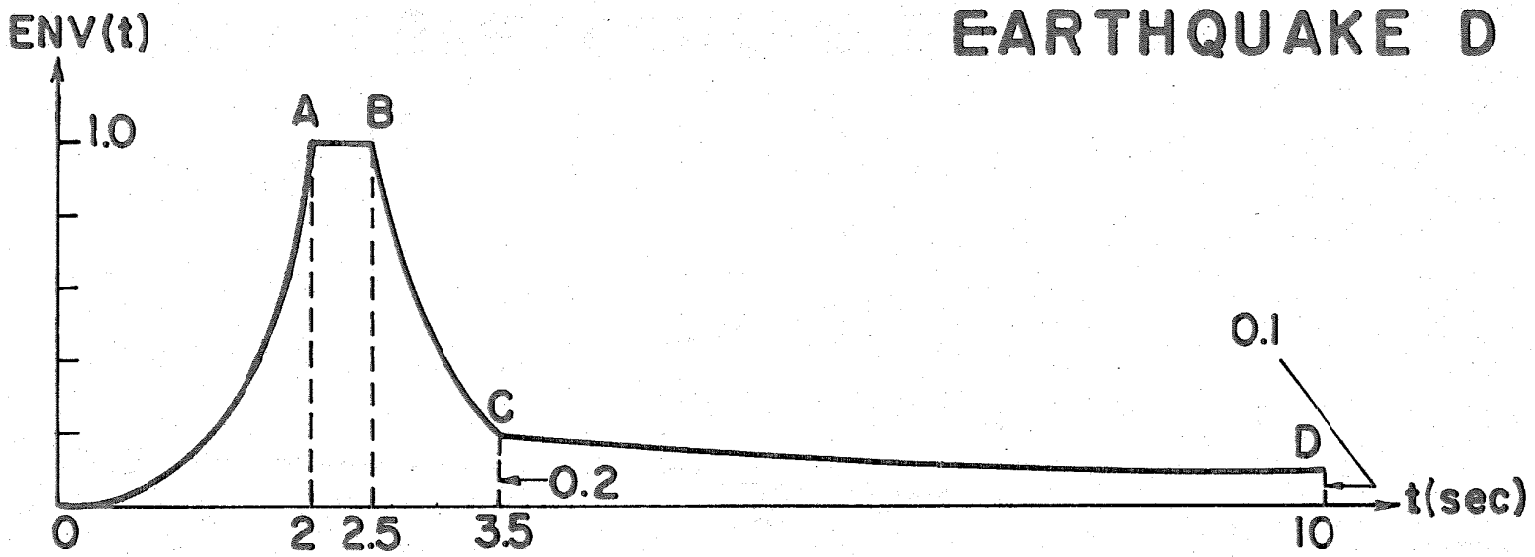

$OA: ENV(t) = t^3/8$

$AB: \quad 1.0$

$BC: \quad \exp[-1.606(t-2.5)]$

$CD: \quad 0.1 + 0.00237(10-t)^2$

Figure 4

Envelope function for earthquake type D

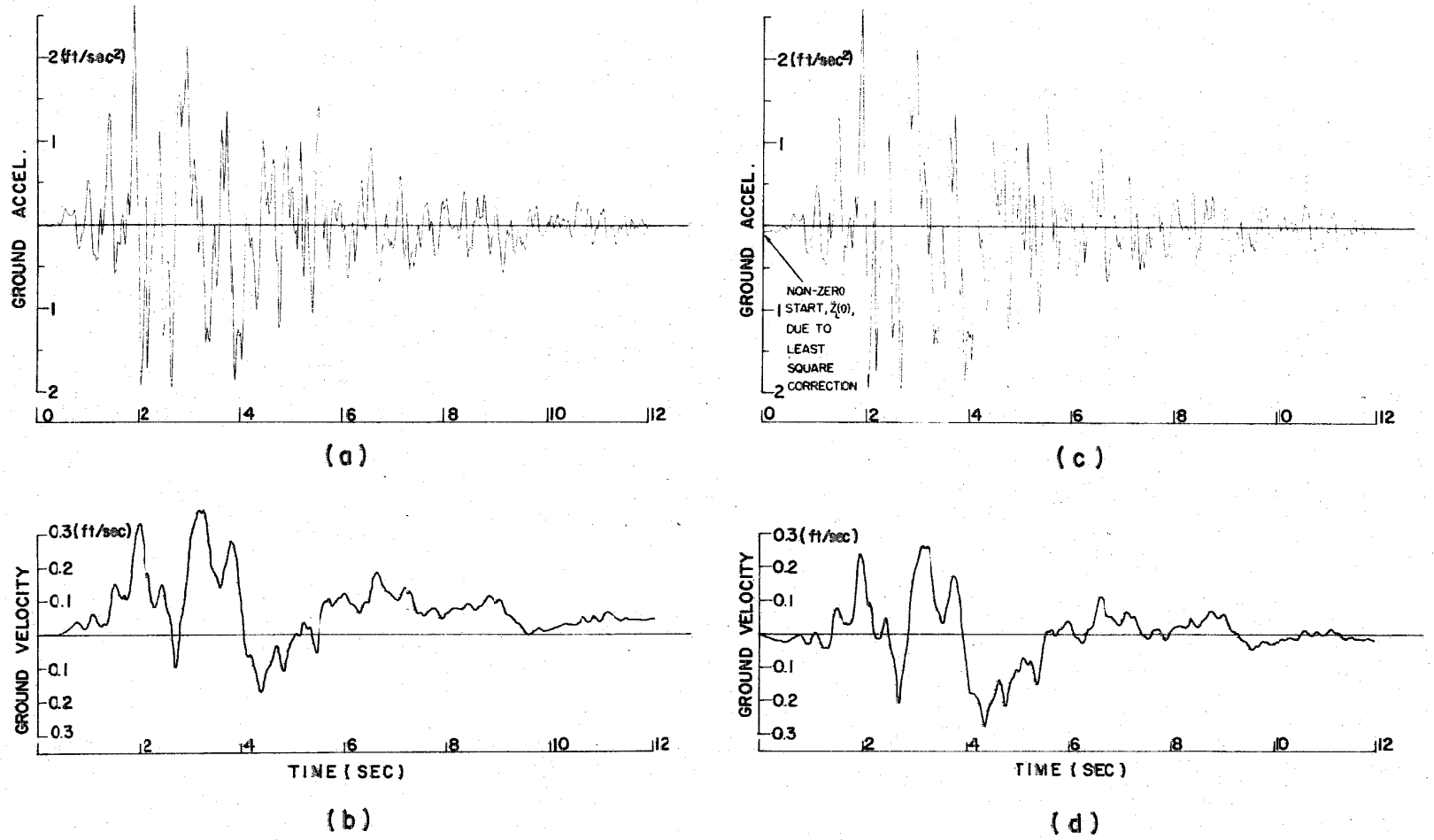

Figure 5

Effects of least square adjustment on earthquake C-1. a) Unadjusted acceleration; b) unadjusted velocity; c) adjusted acceleration; and d) adjusted velocity

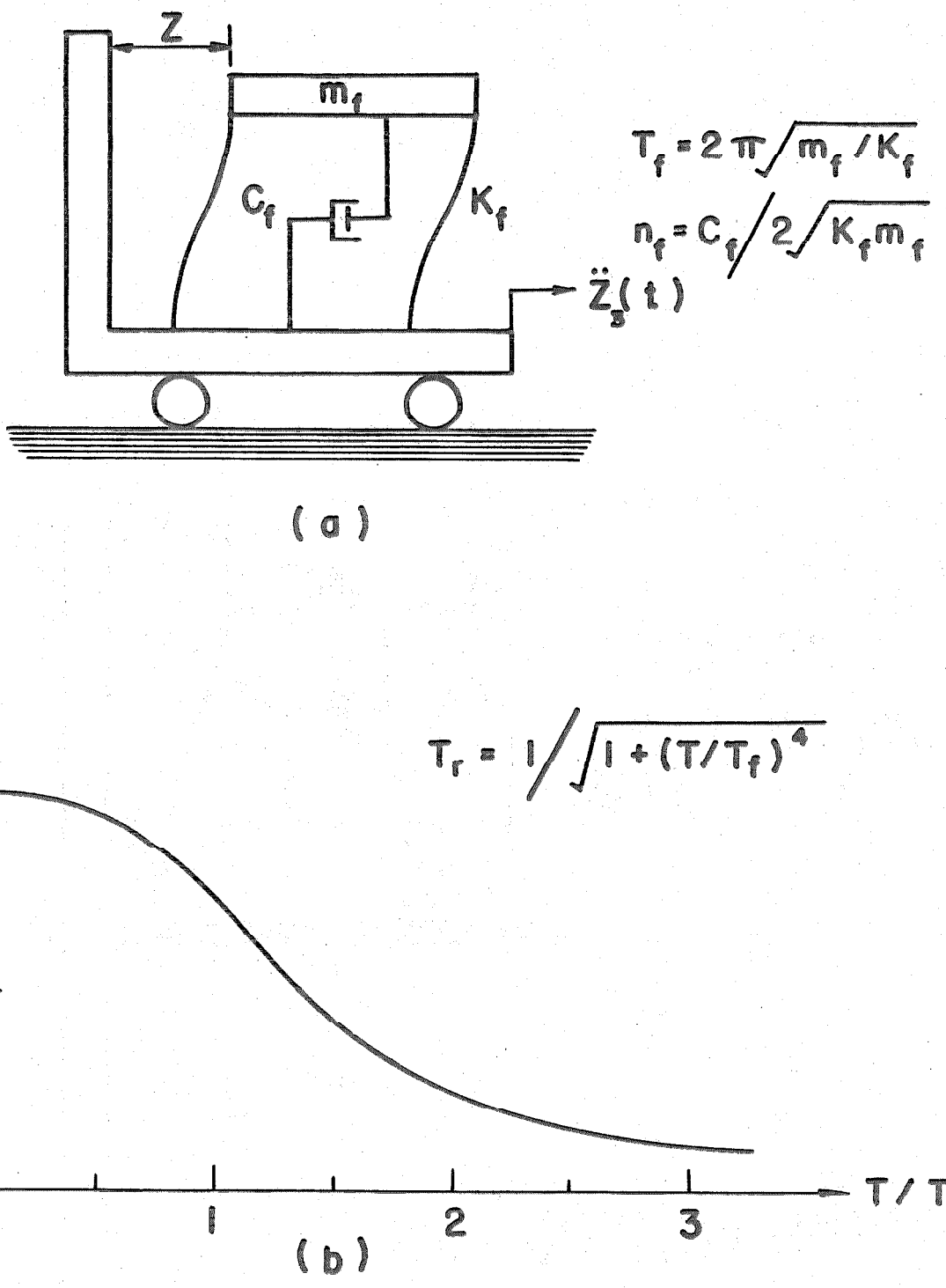

Figure 6

Second order filter used to attenuate long period components of the accelerograms. a) Physical model of filter; and b) Filter transfer function

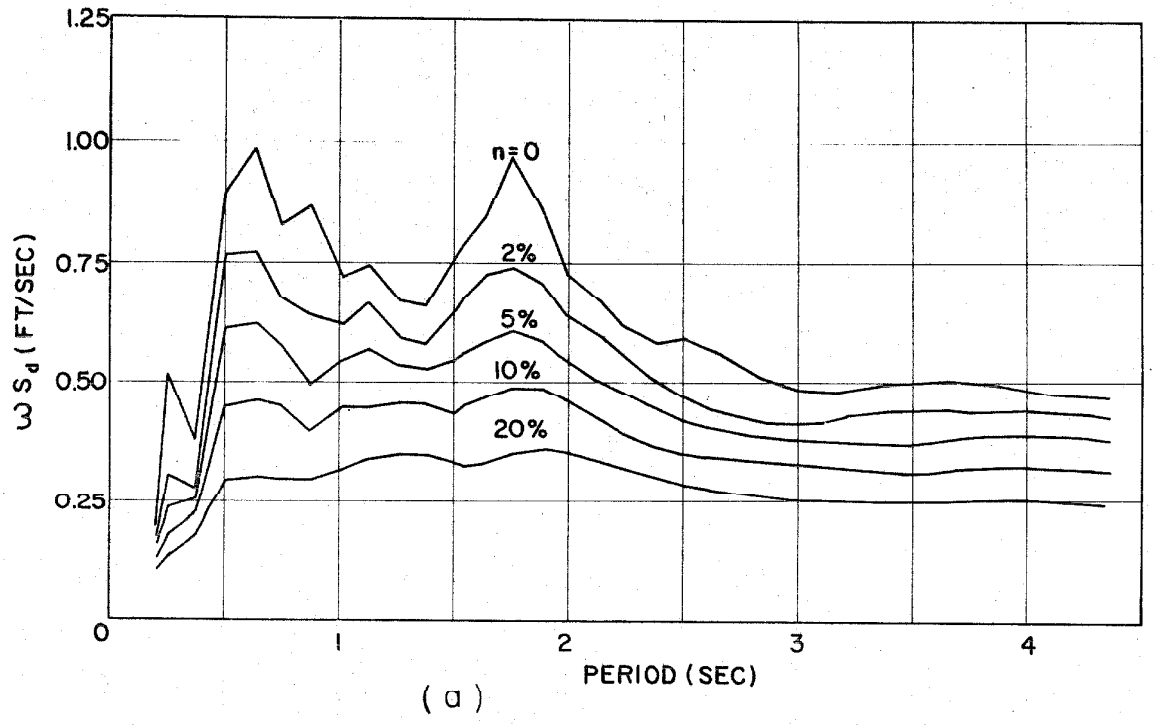

(a)

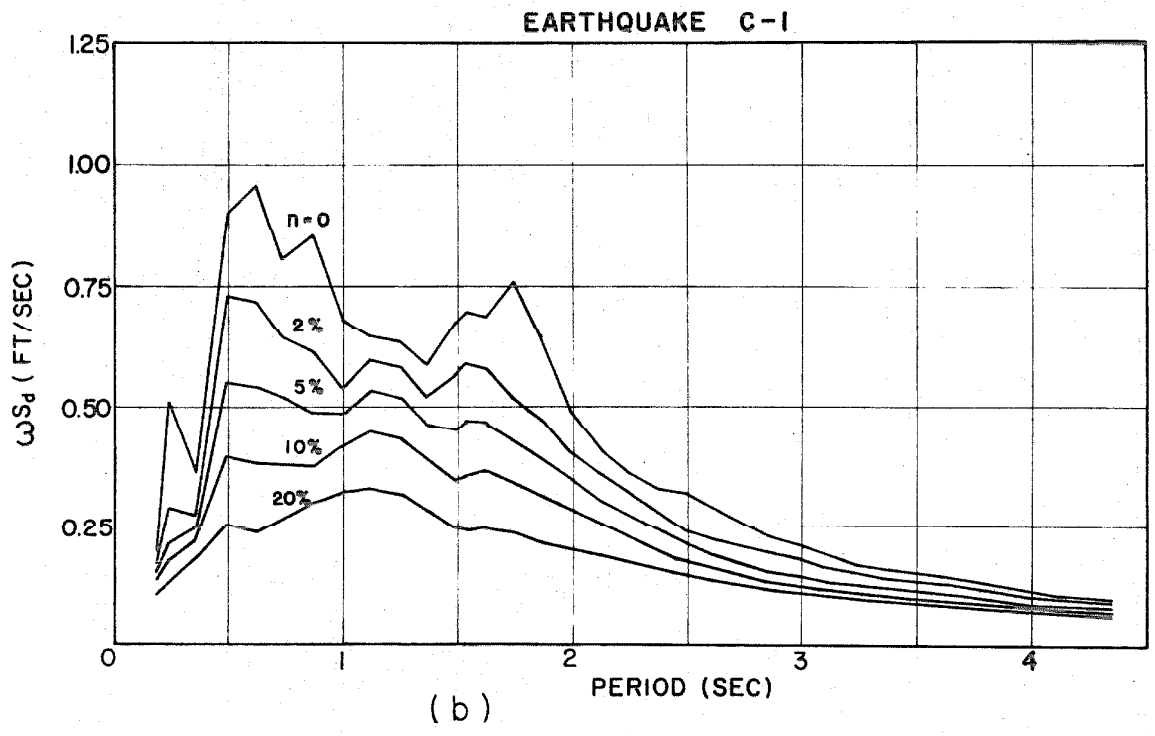

(b)

Figure 7

Effects of filtering on the spectrum of earthquake C-1. a) Before filtering; and b) After filtering with T_f = 2 seconds

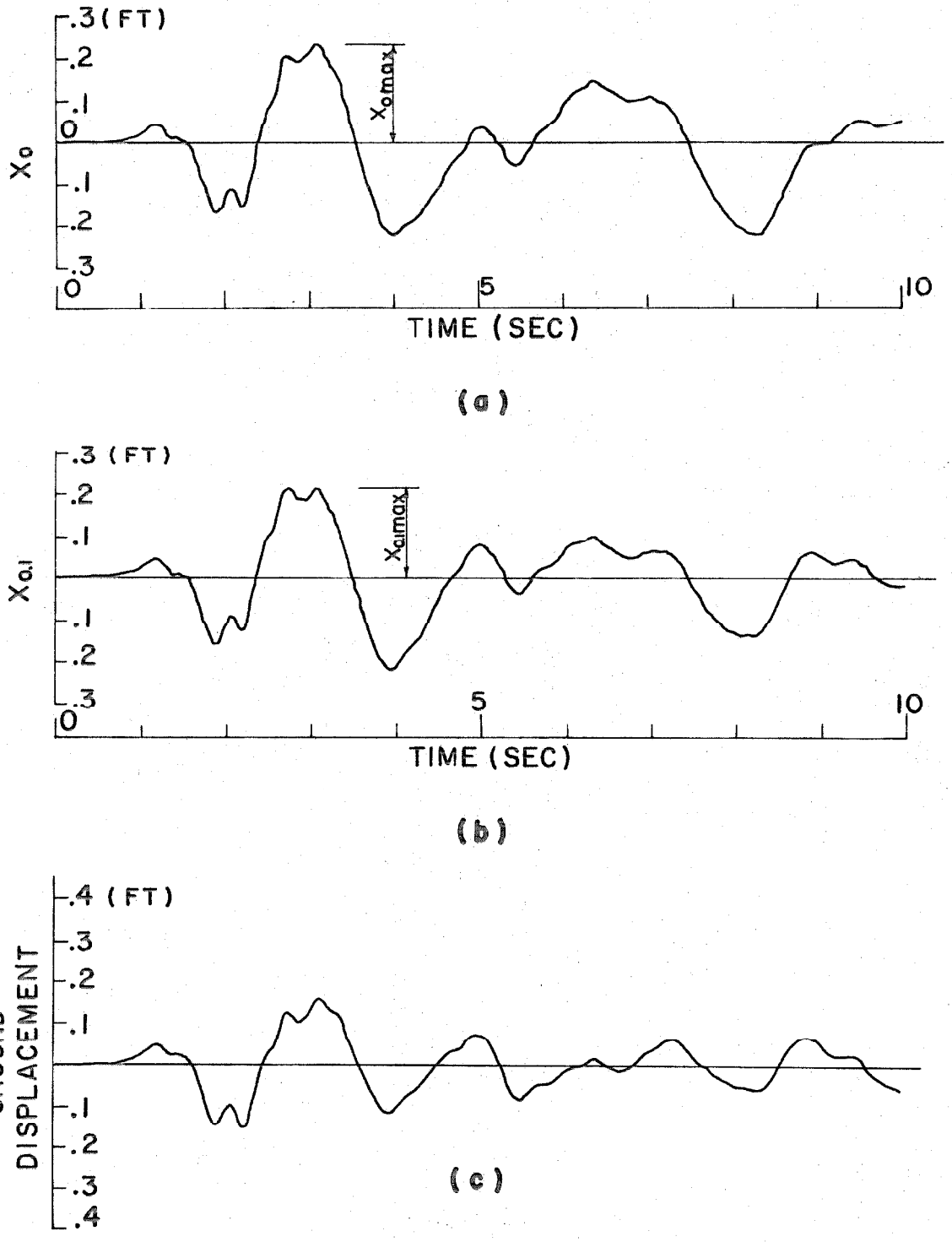

Figure 8

Response of 4 second period oscillator to earthquake D-1. a) Undamped response; b) 10 percent damped response; and c) ground displacement

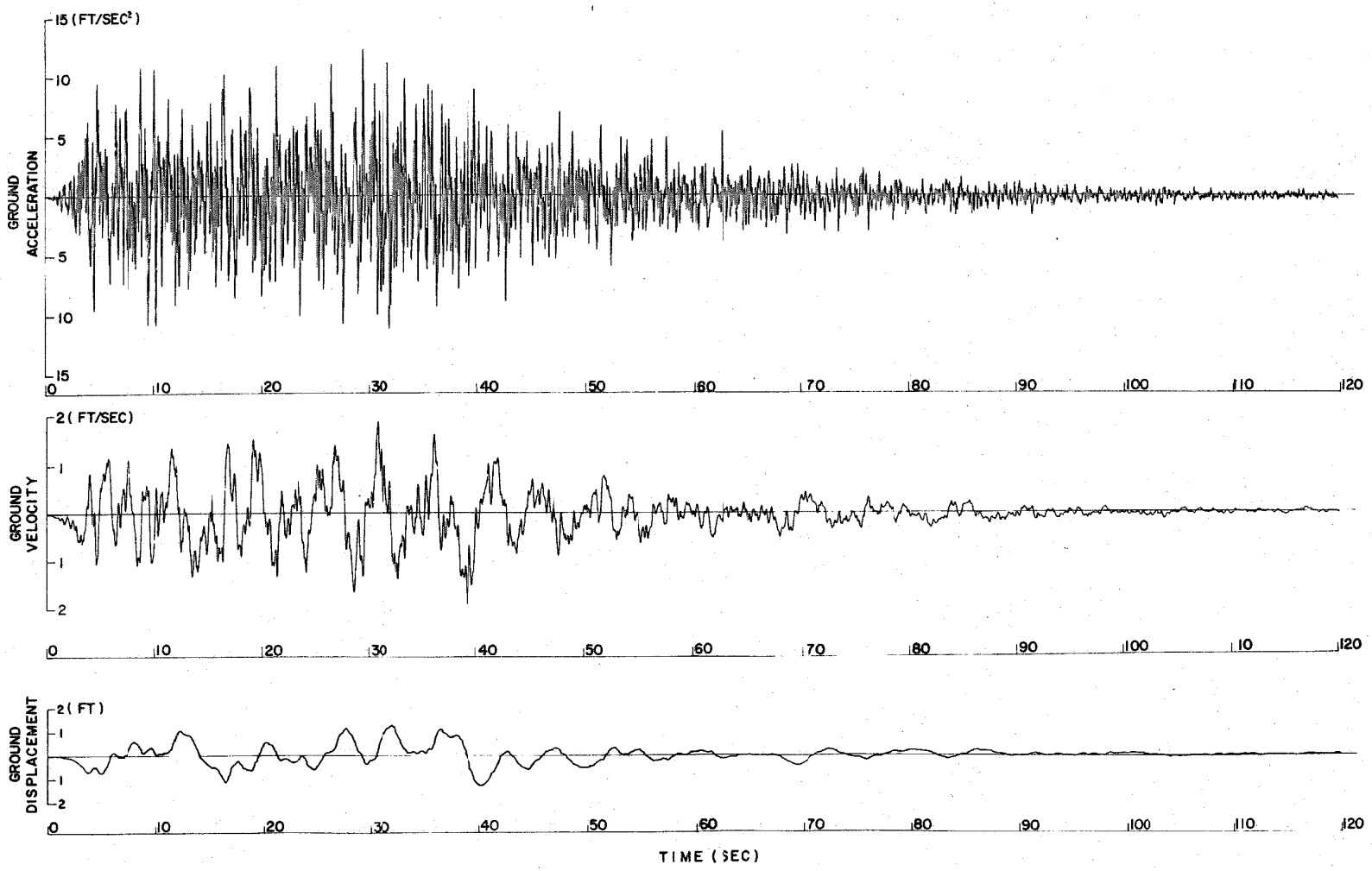

EARTHQUAKE A-1

Figure 9

Acceleration, velocity and displacement for earthquake A-1

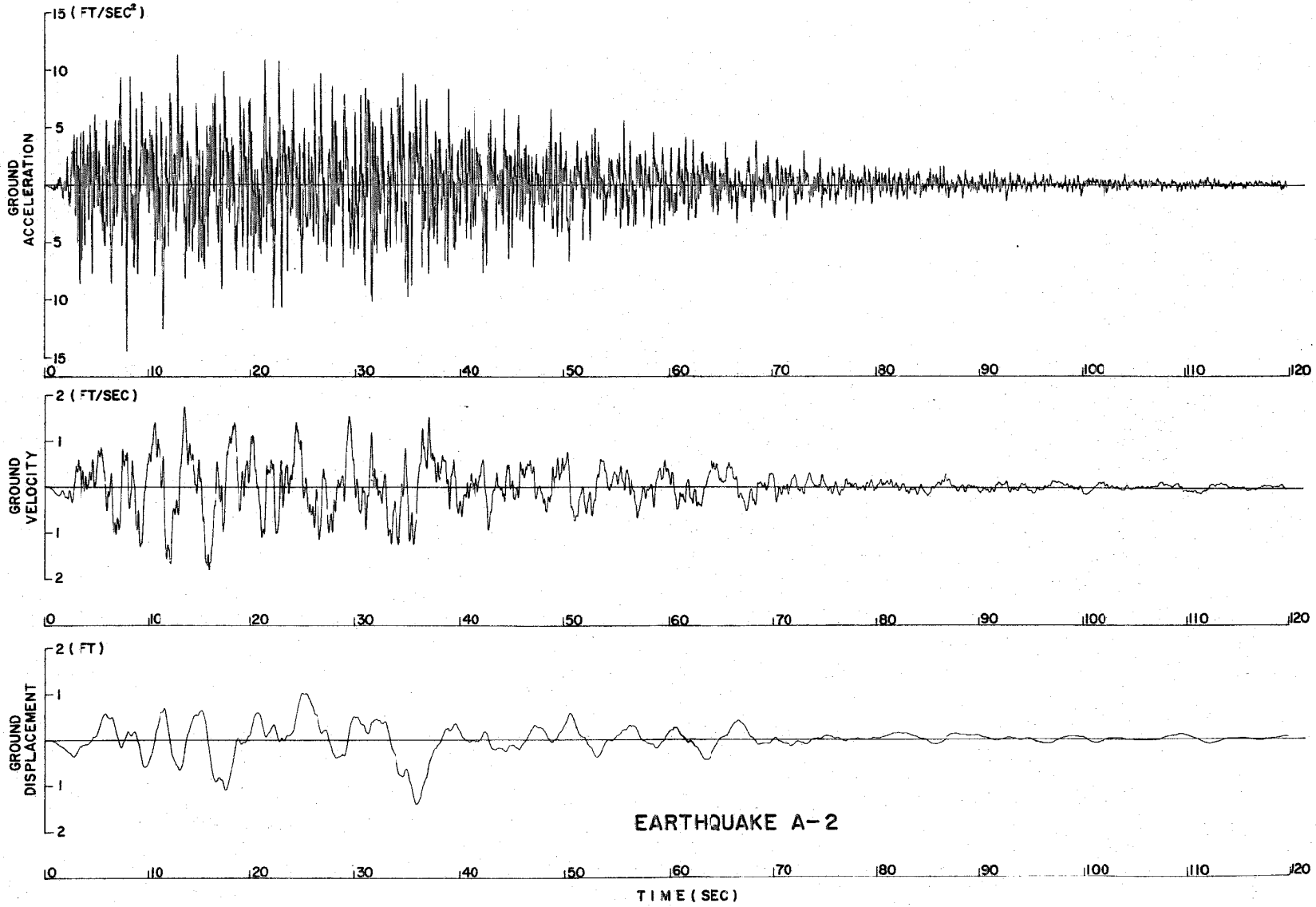

Figure 10

Acceleration, velocity and displacement for earthquake A-2

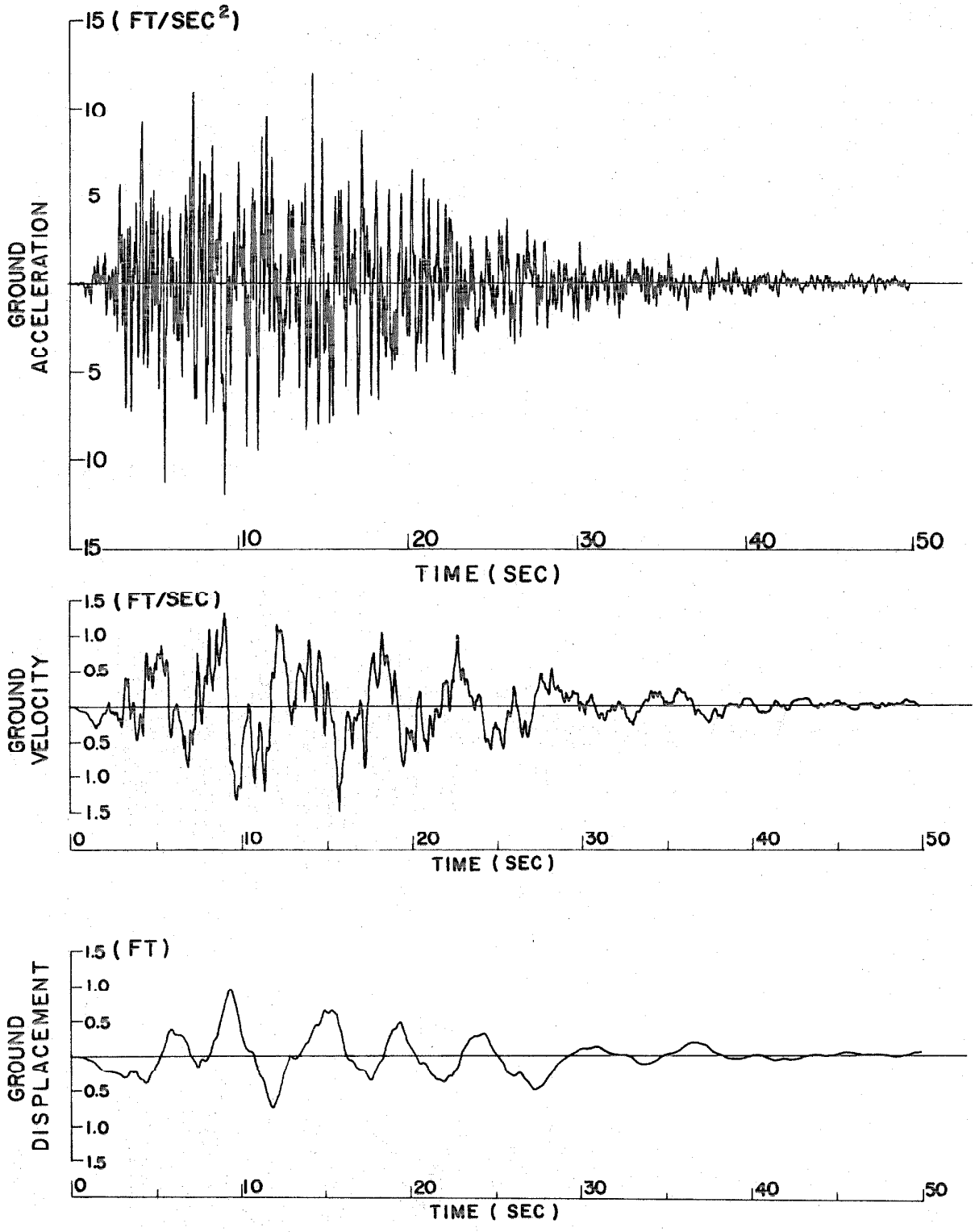

EARTHQUAKE B-1

Figure 11

Acceleration, velocity and displacement for earthquake B-1

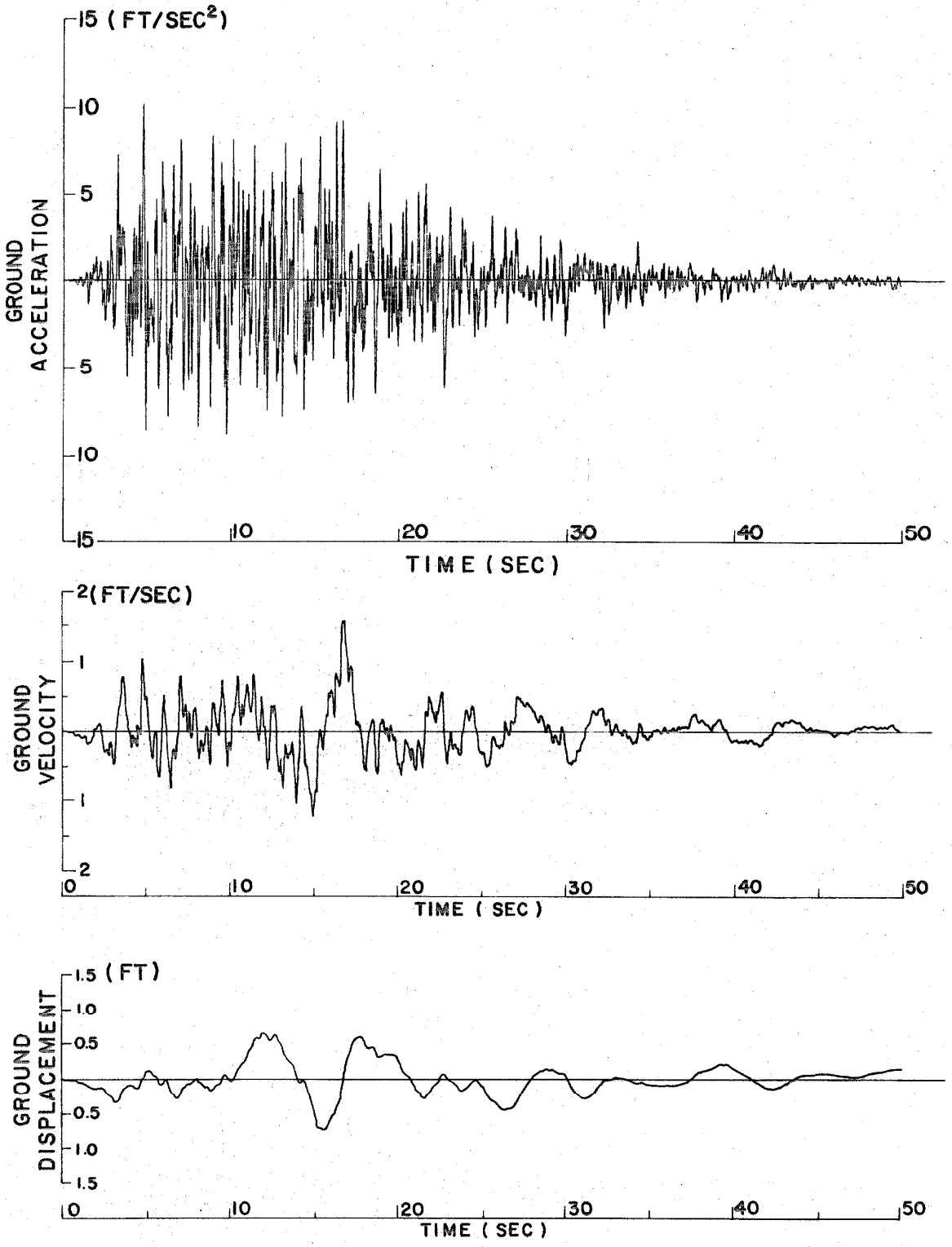

EARTHQUAKE B-2

Figure 12

Acceleration, velocity and displacement for earthquake B-2

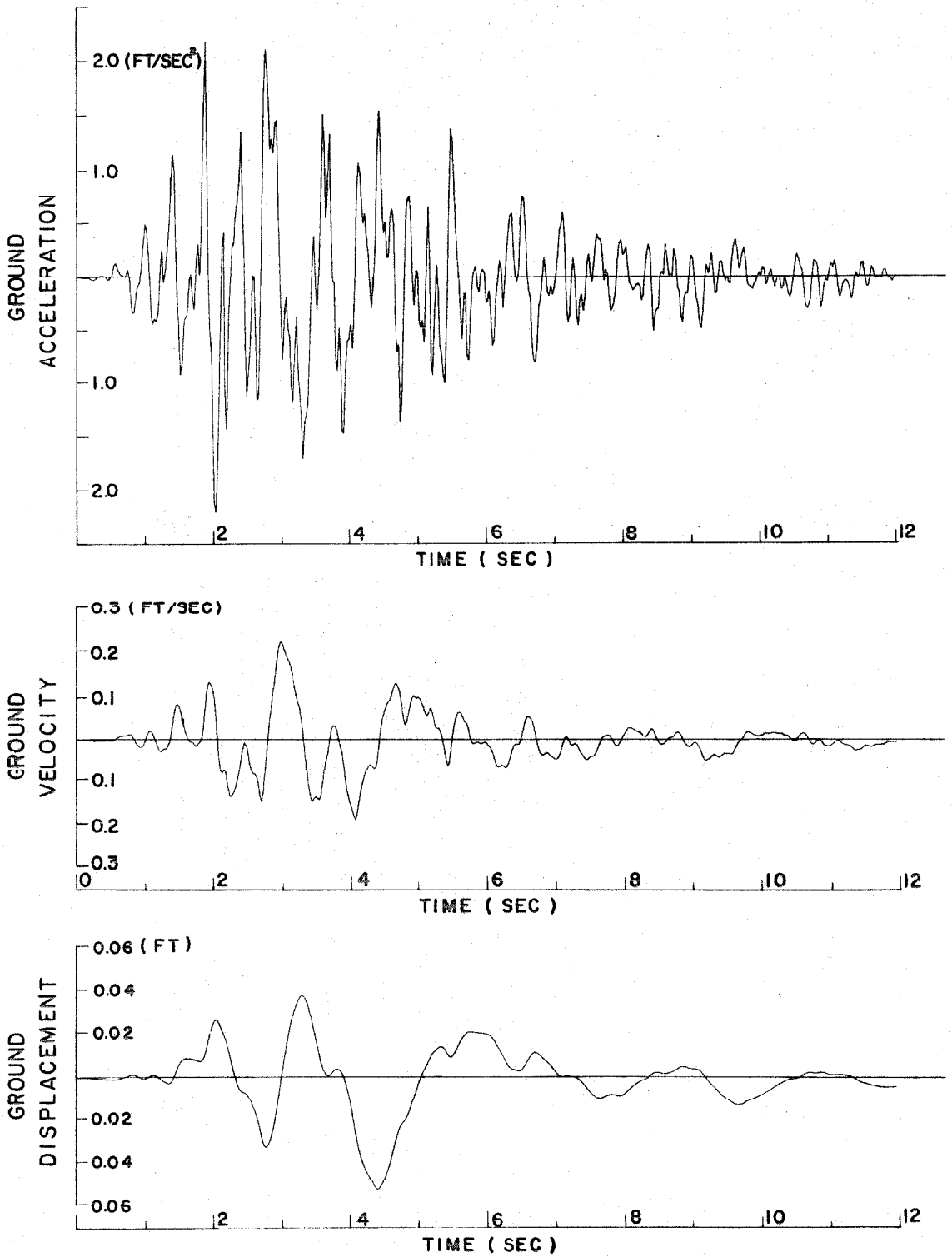

EARTHQUAKE C-1

Figure 13

Acceleration, velocity and displacement for earthquake C-1

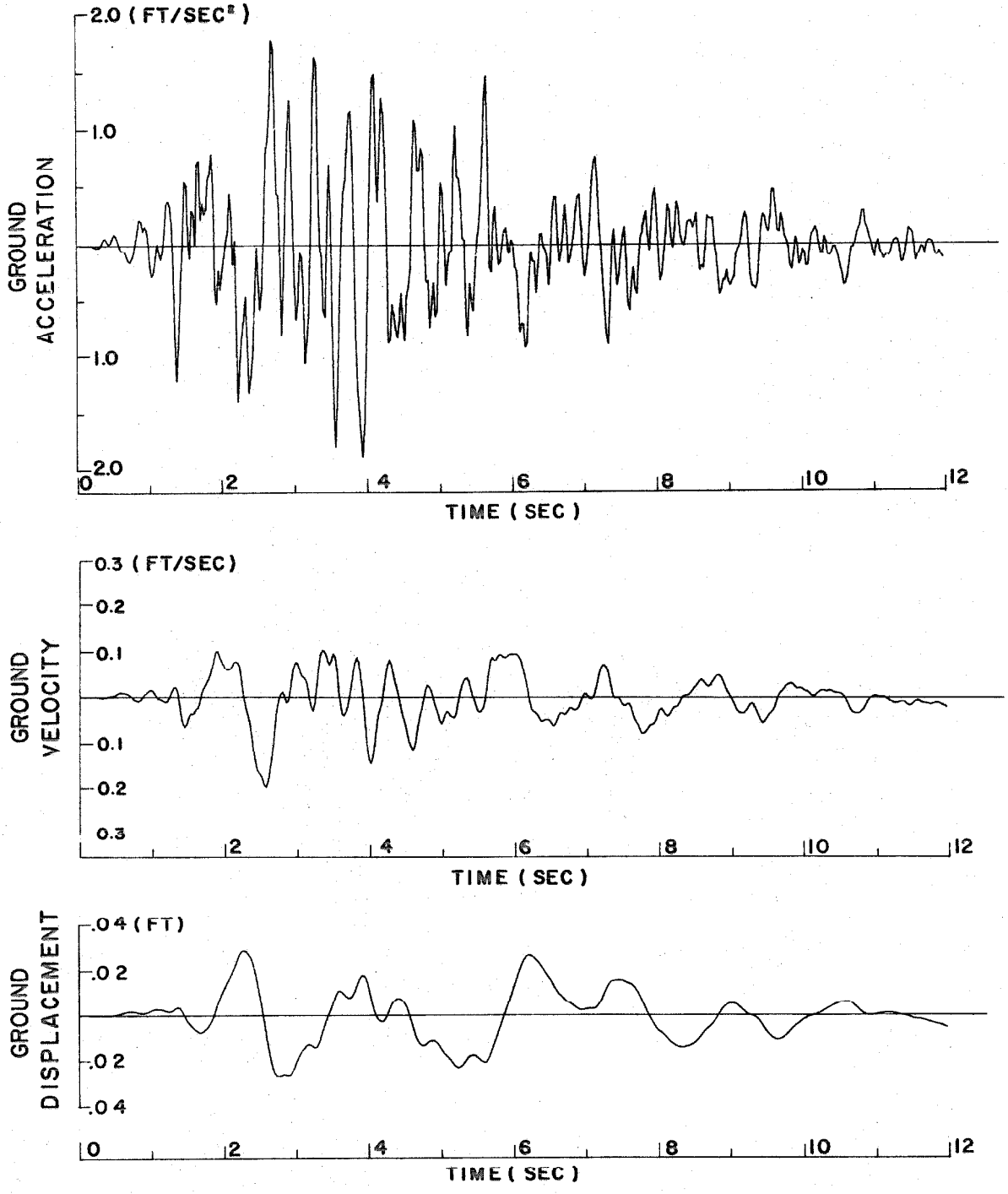

EARTHQUAKE C-2

Figure 14

Acceleration, velocity and displacement for carthquake C-2

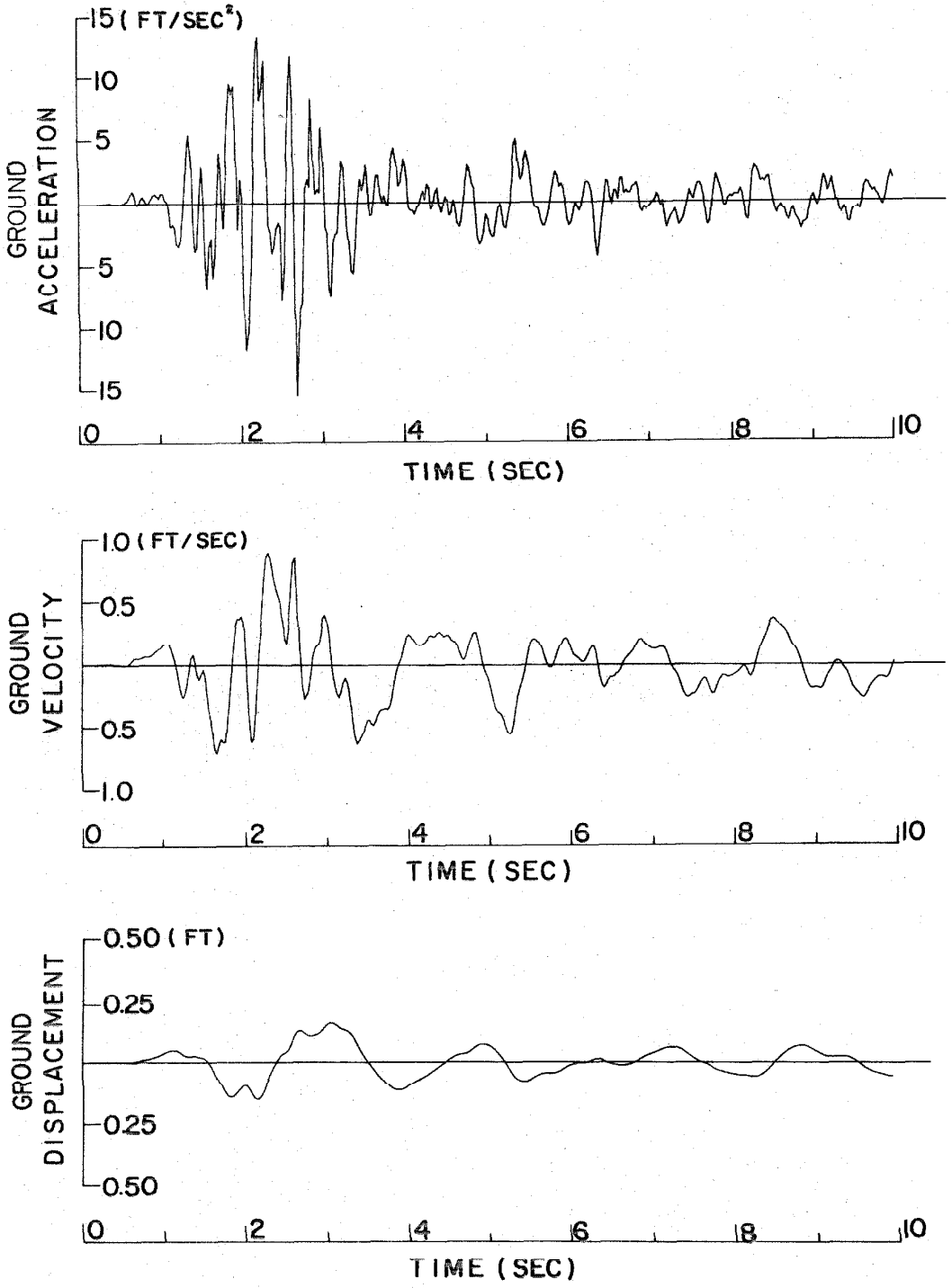

EARTHQUAKE D-1

Figure 15

Acceleration, velocity and displacement for earthquake D-1

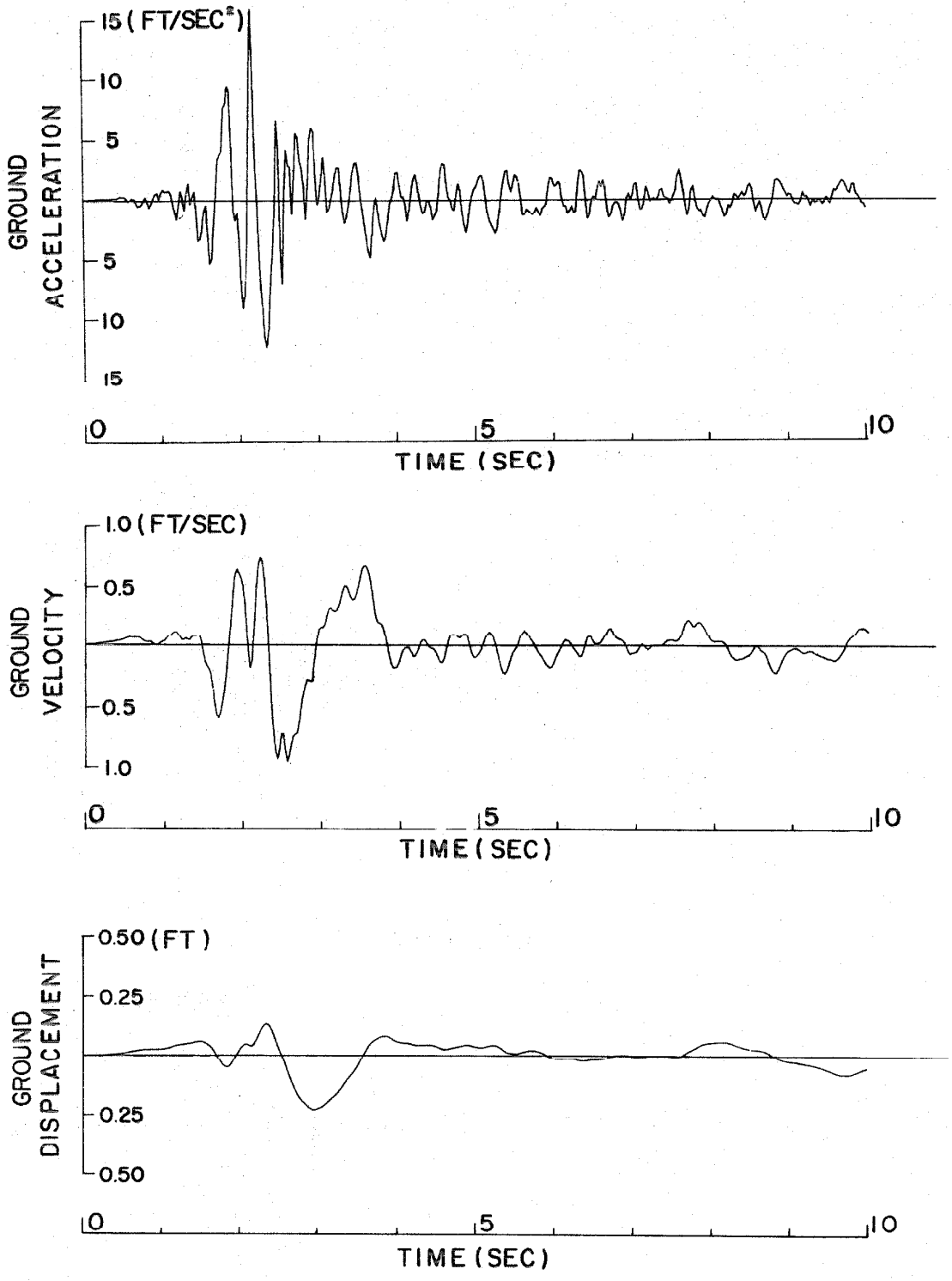

EARTHQUAKE D-2

Figure 16

Acceleration, velocity and displacement for earthquake D-2

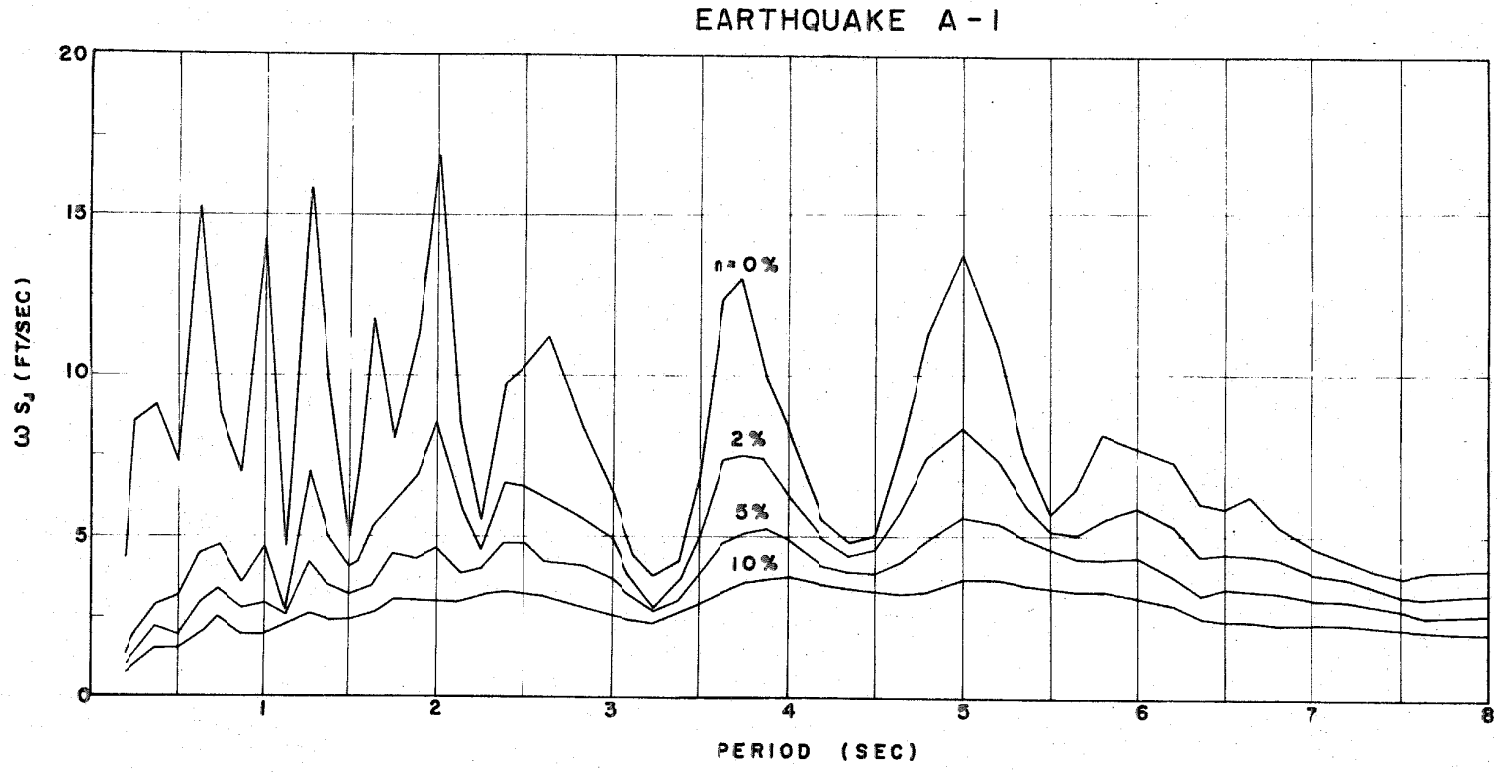

Figure 17

ωS_d spectrum for earthquake A-1

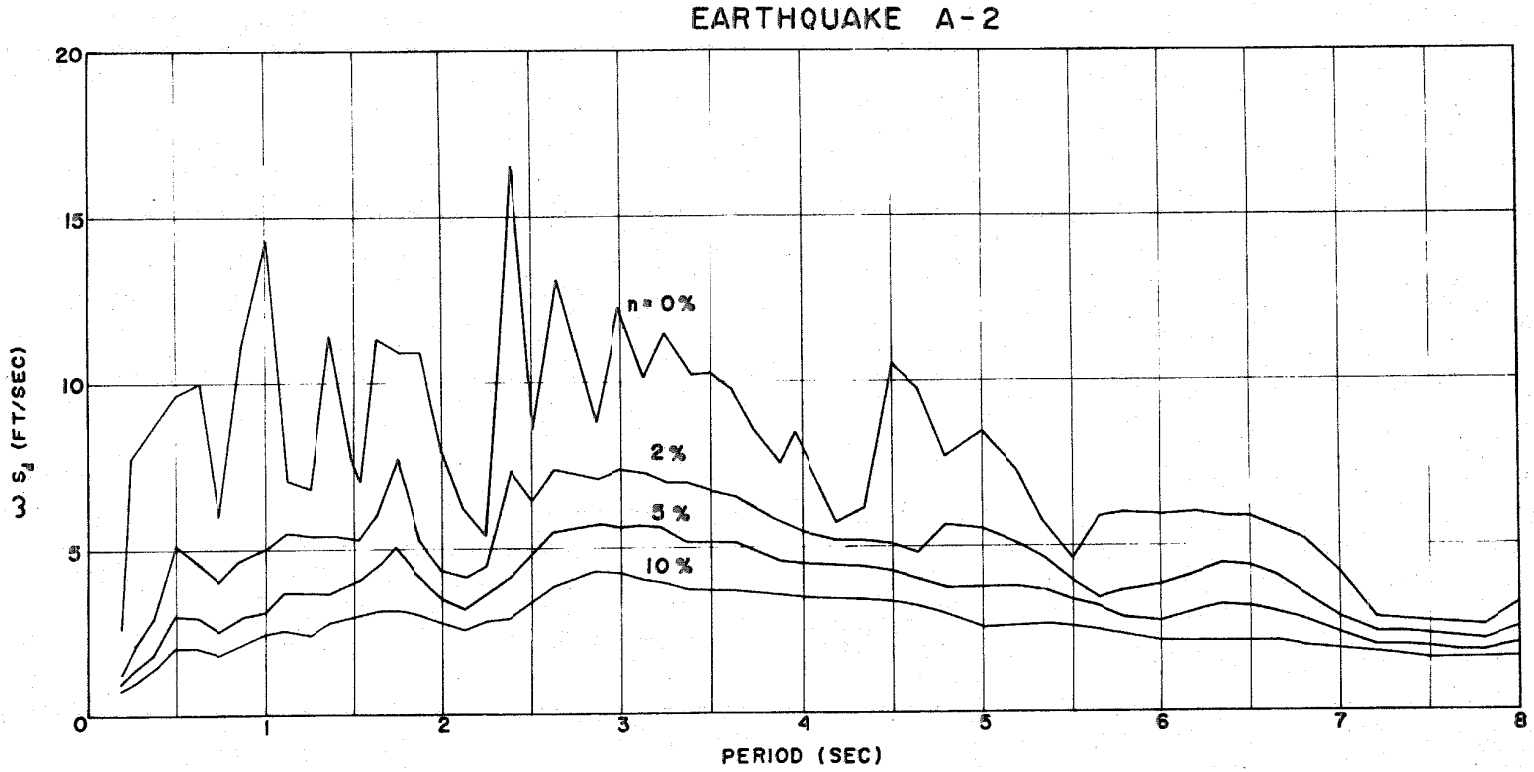

Figure 18

ωS_d spectrum for earthquake A-2

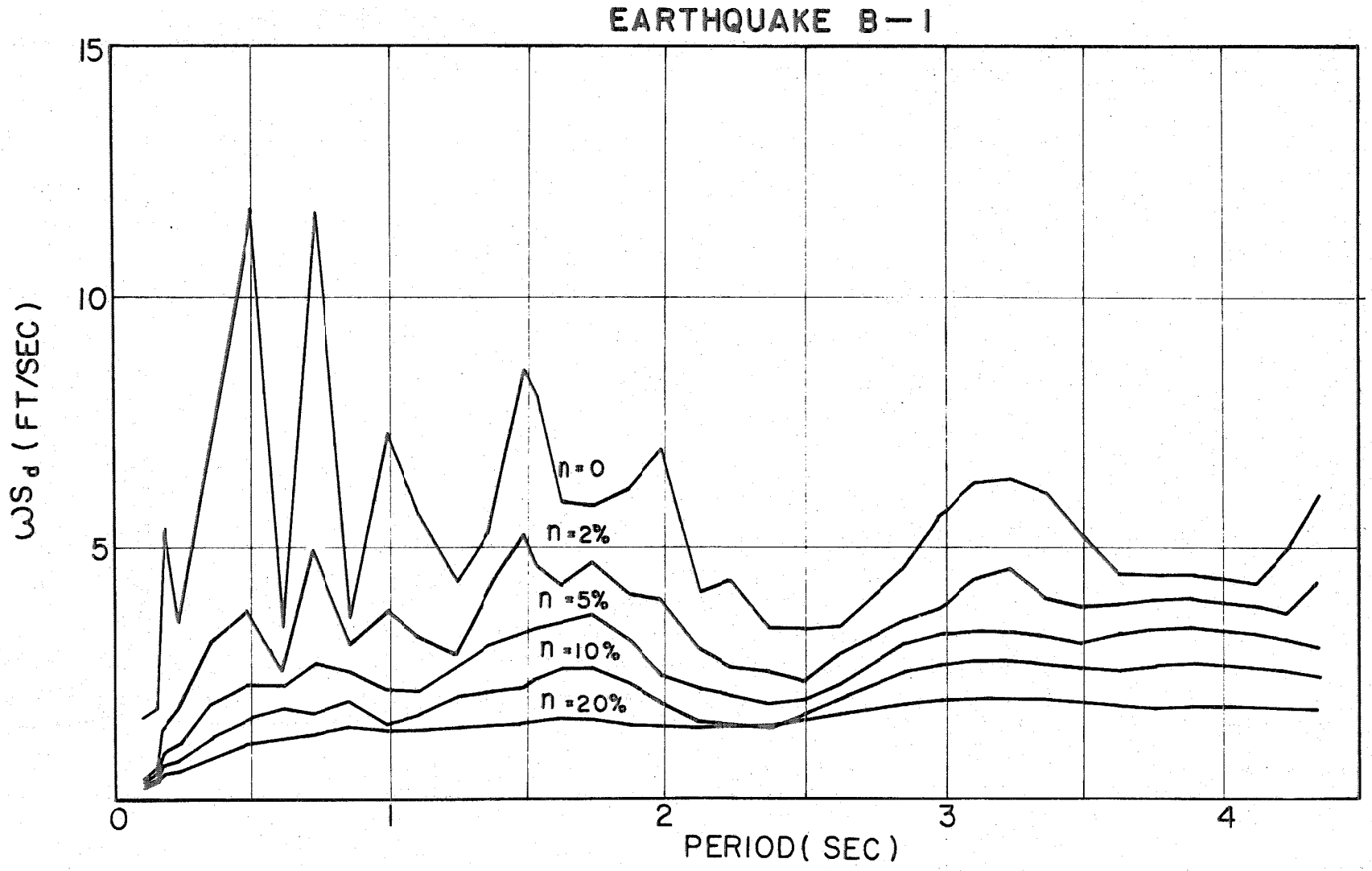

Figure 19

ωS_d spectrum for earthquake B-1

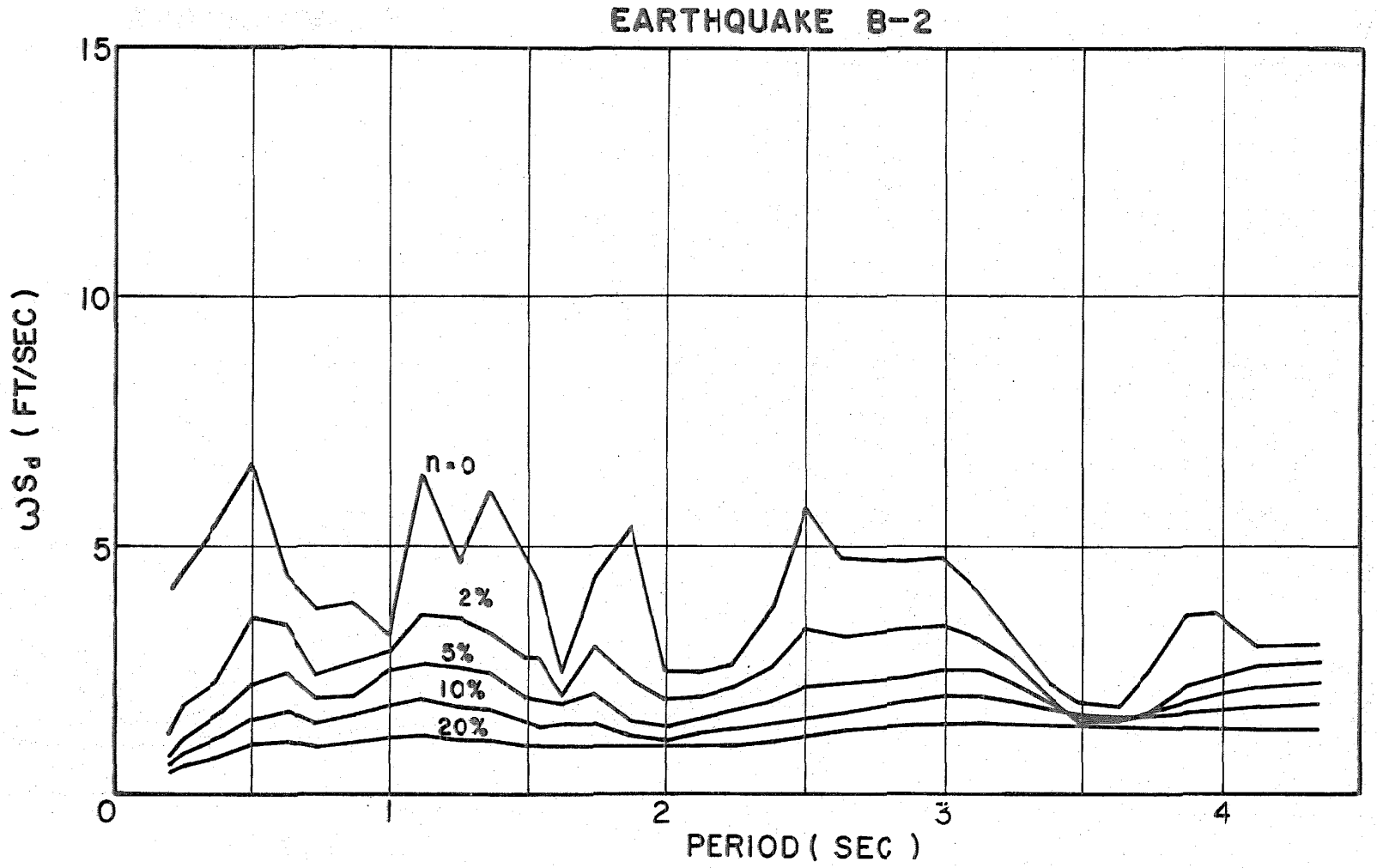

Figure 20

ωS_d spectrum for earthquake B-2

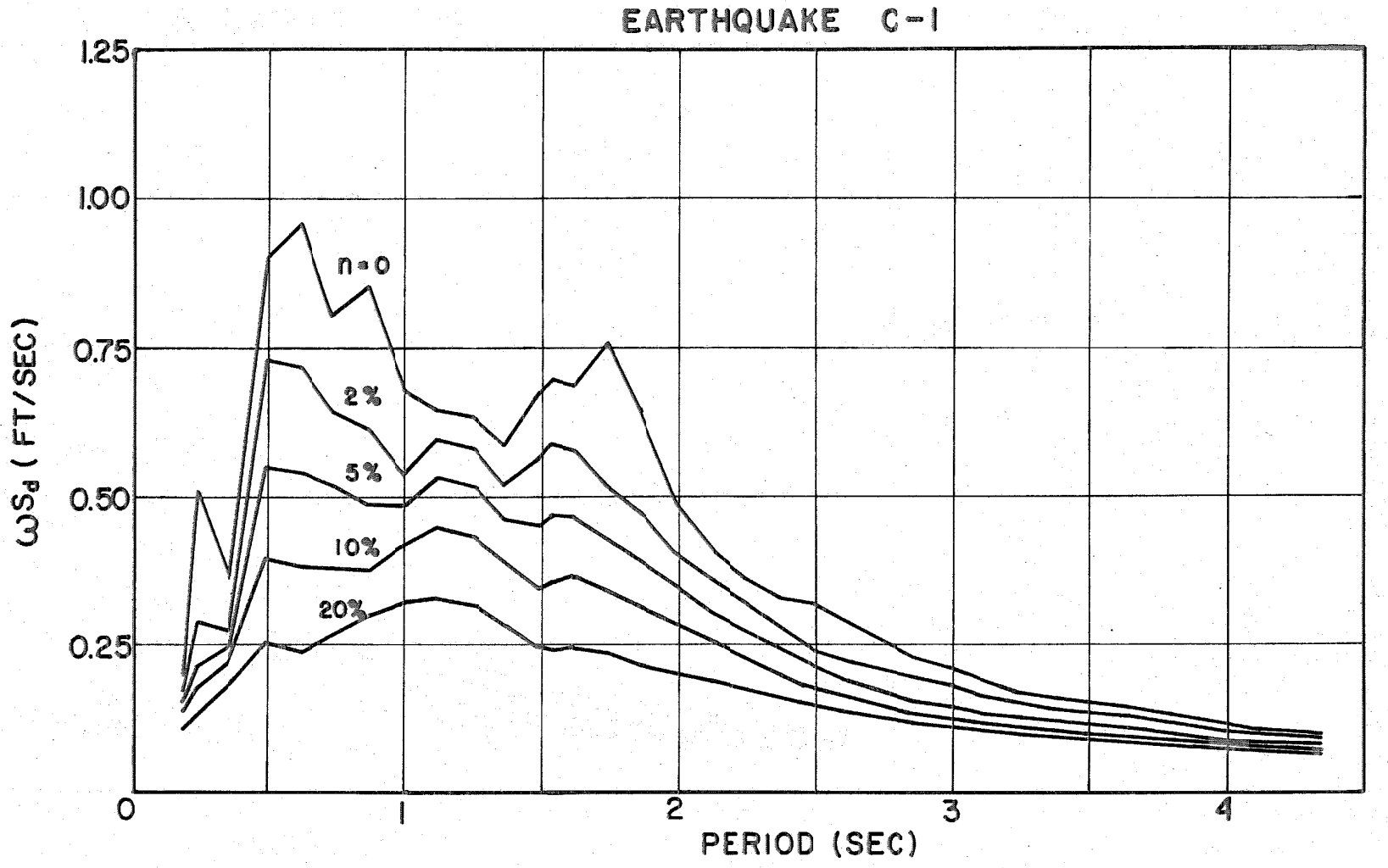

Figure 21

ωS_d spectrum for earthquake C-1

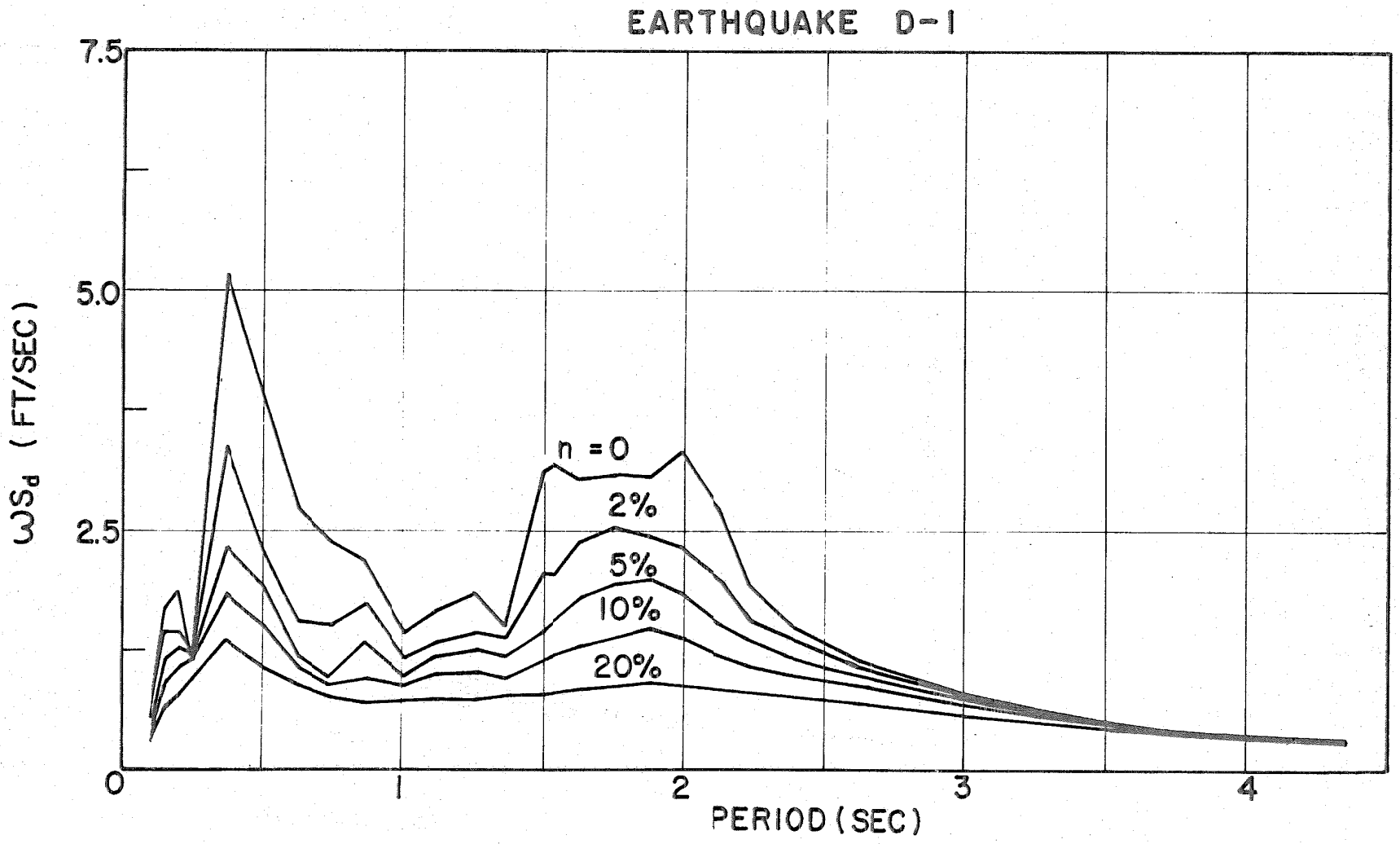

Figure 23

ωS_d spectrum for earthquake D-1

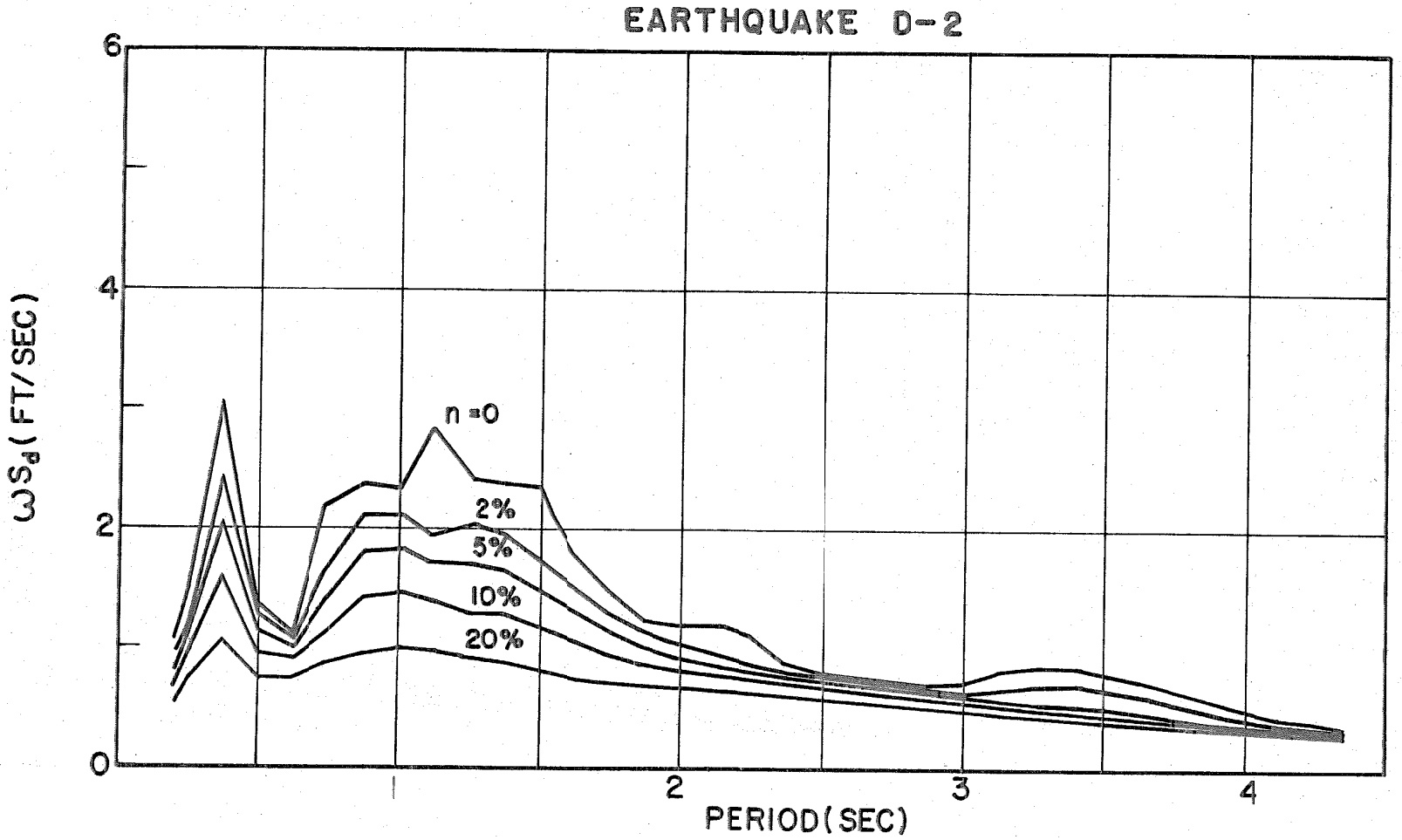

Figure 24

ωS_d spectrum for earthquake D-2

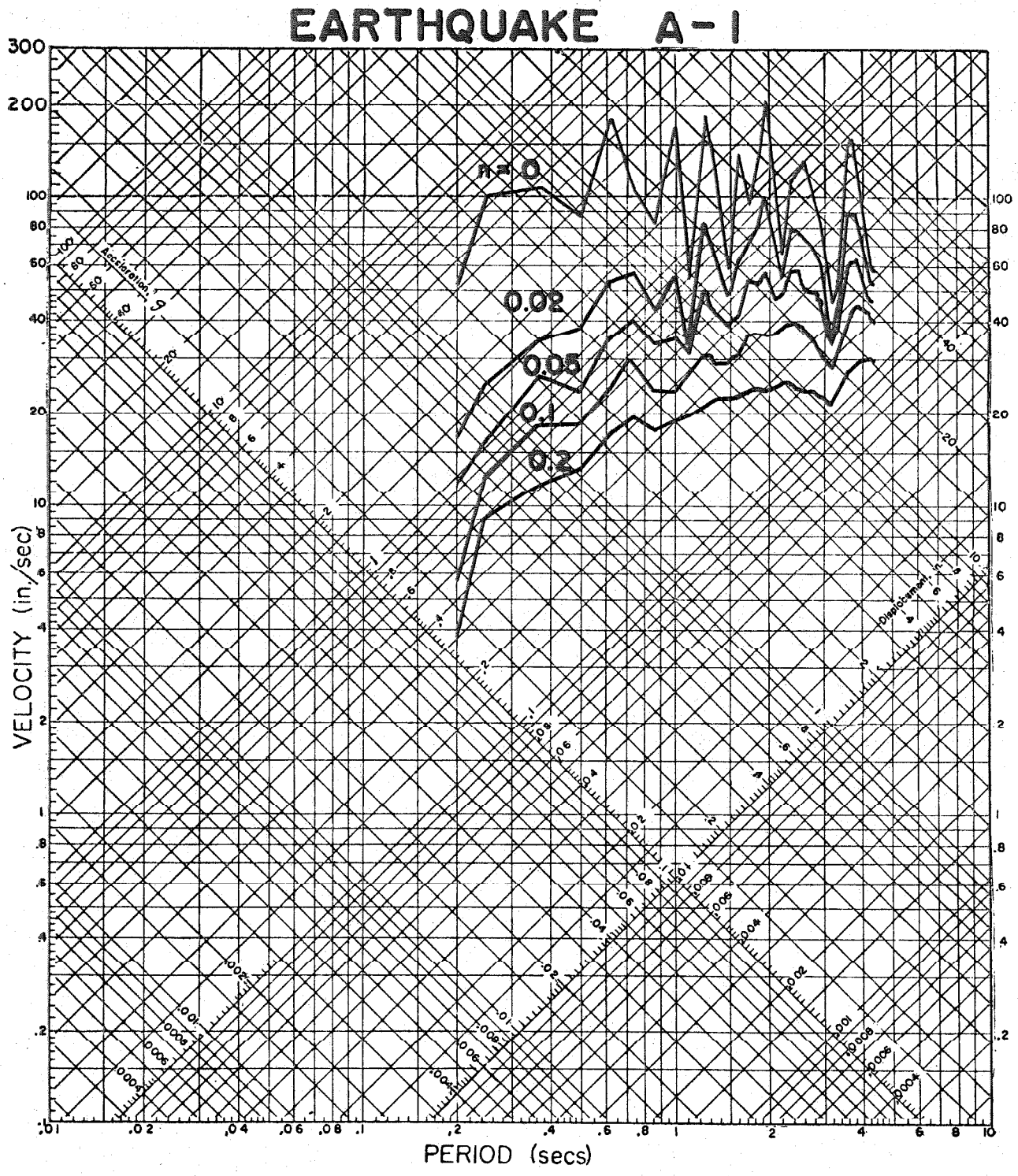

Figure 25

Tripartite logarithmic plot of spectra for earthquake A-1

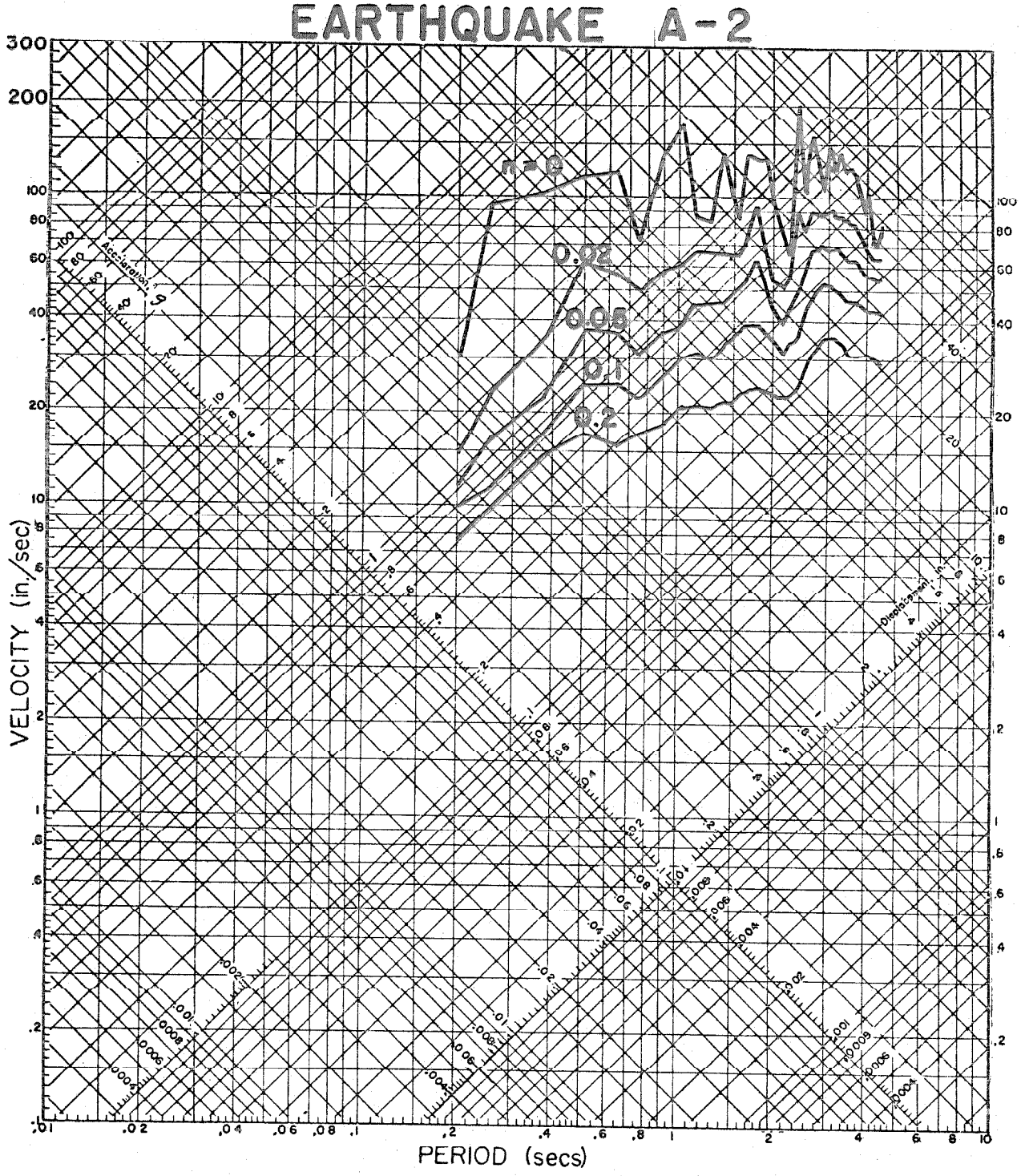

Figure 26

Tripartite logarithmic plot of spectra for earthquake A-2

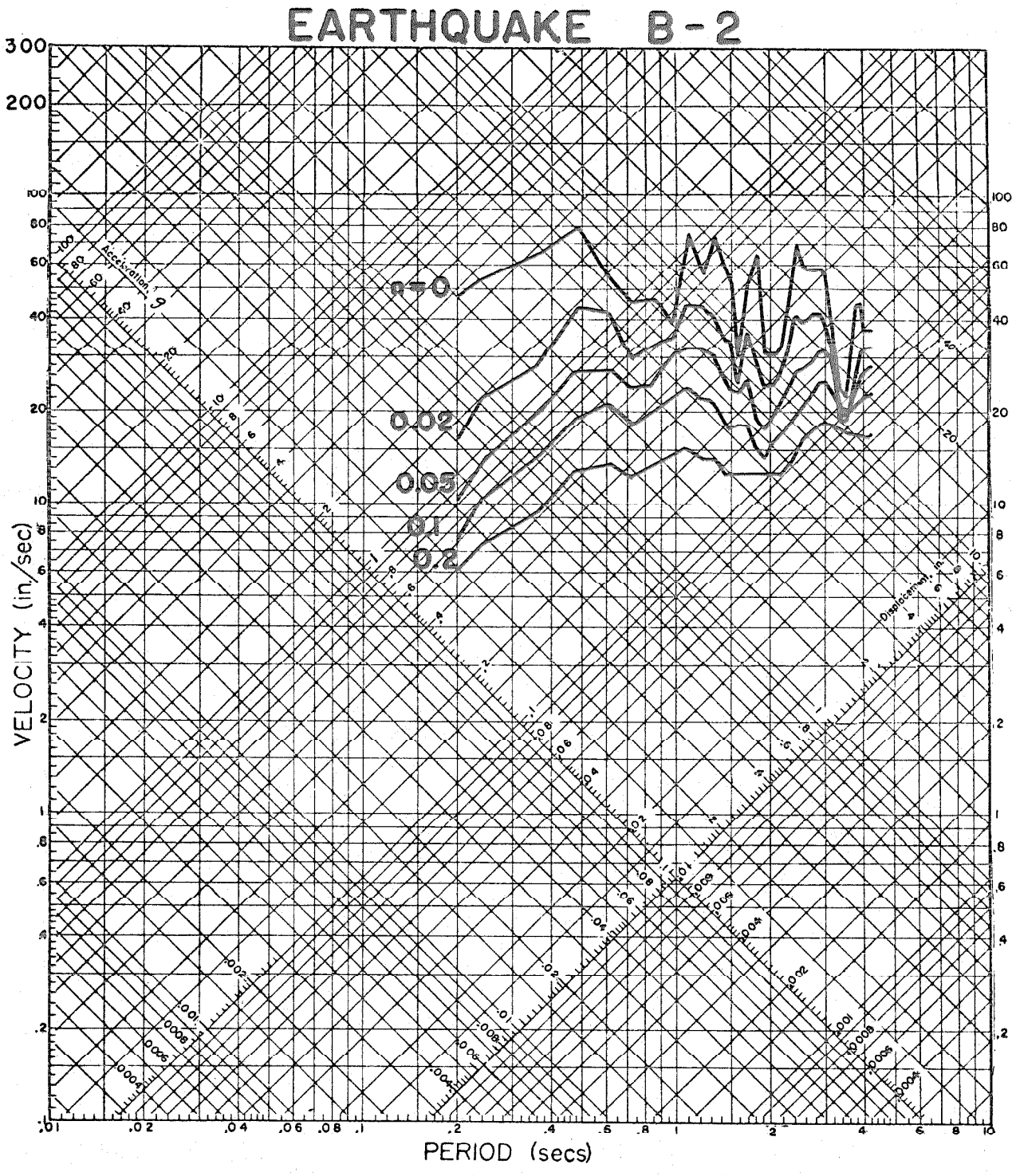

Figure 28

Tripartite logarithmic plot of spectra
for earthquake B-2

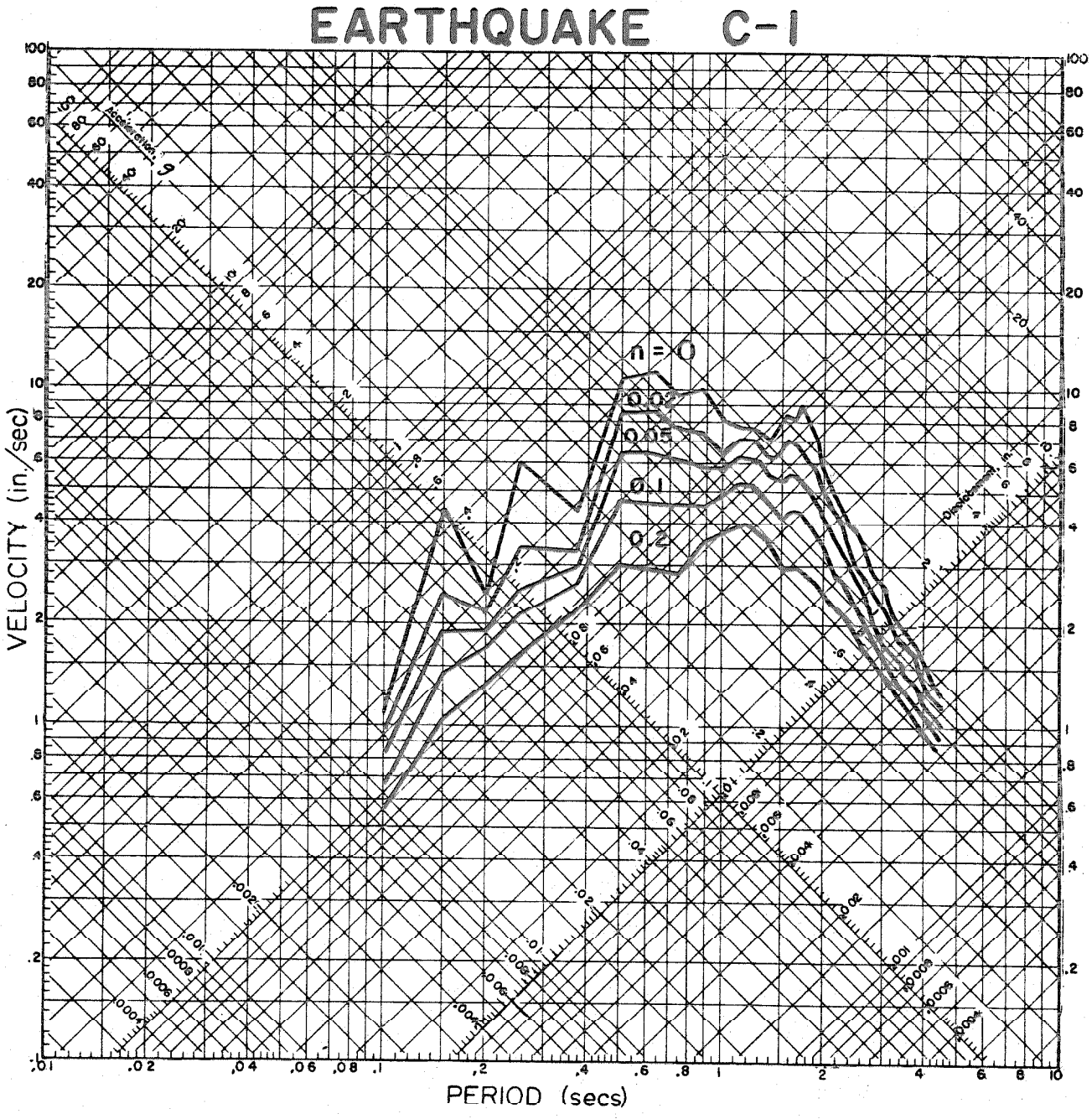

Figure 29

Tripartite logarithmic plot of spectra
for earthquake C-1

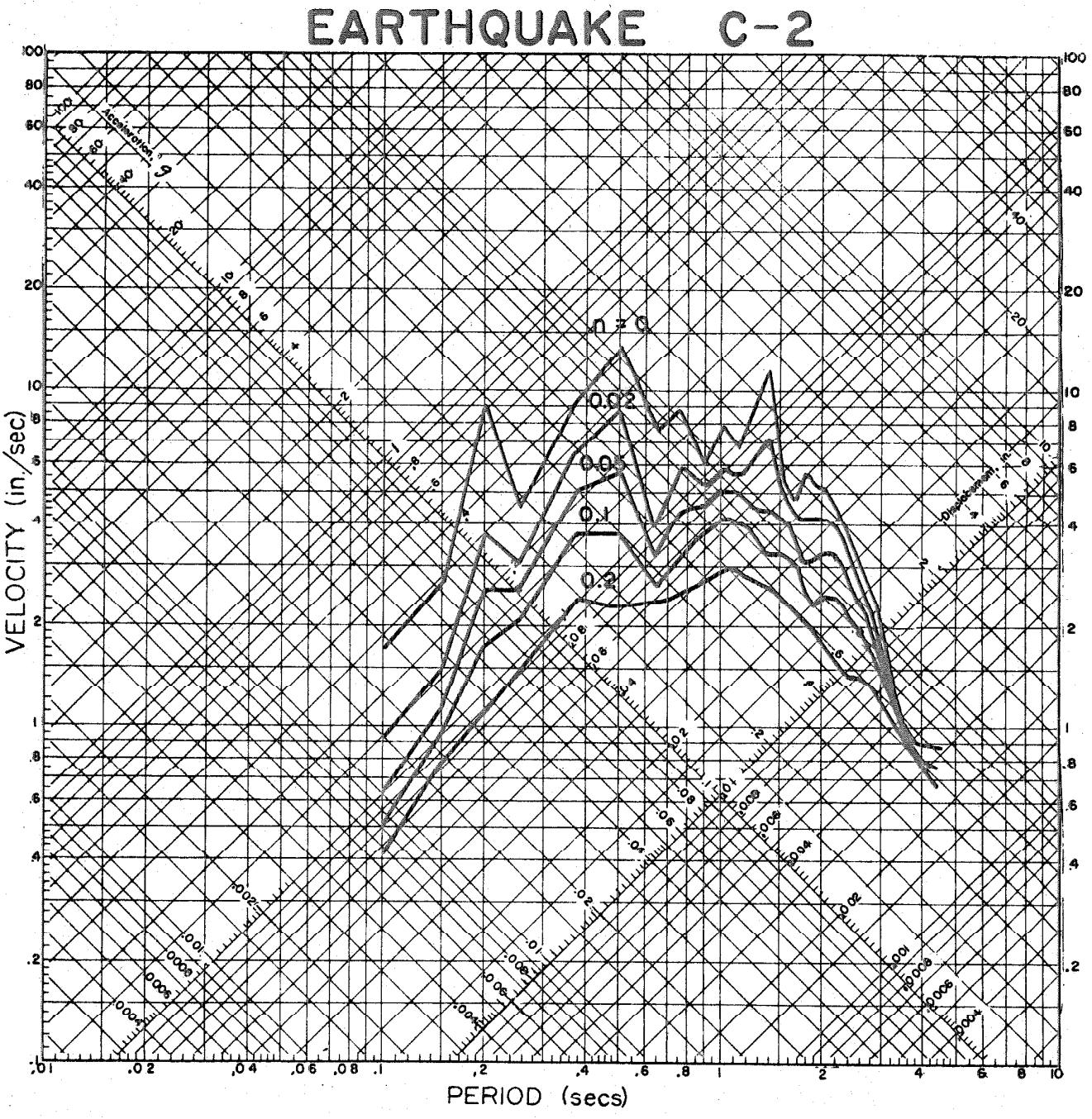

Figure 30

Tripartite logarithmic plot of spectra
for earthquake C-2

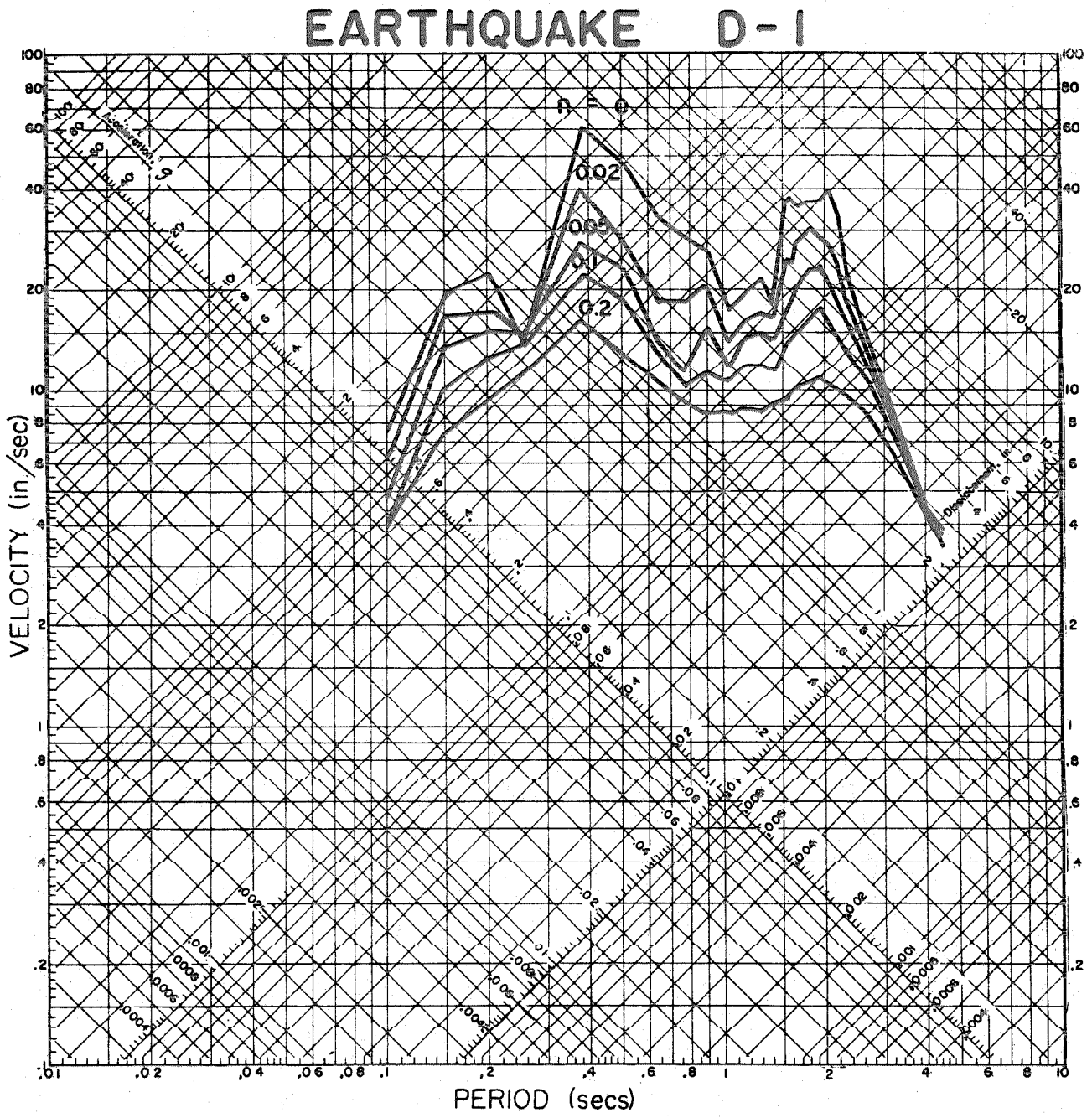

Figure 31

Tripartite logarithmic plot of spectra
for earthquake D-1

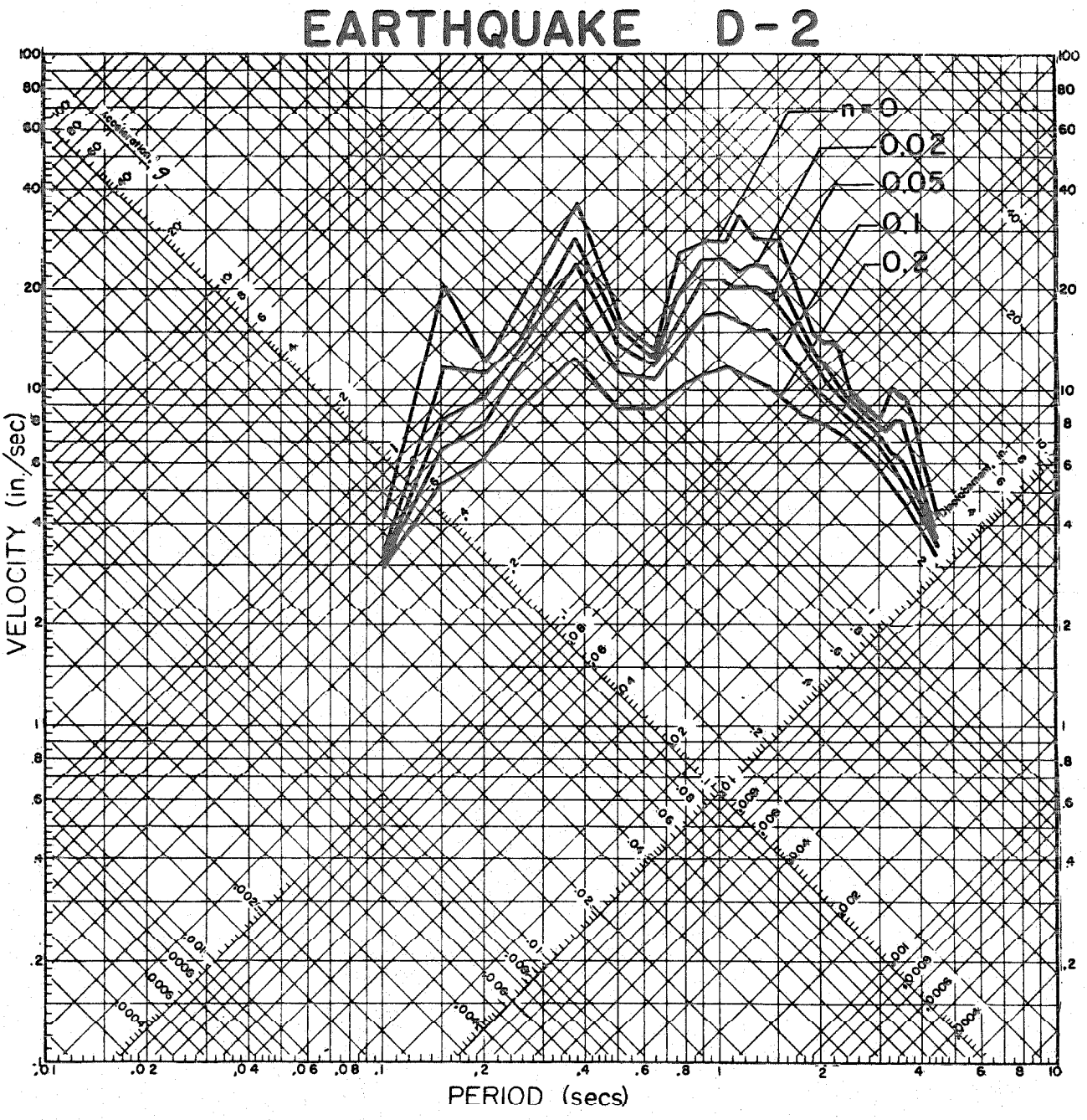

Figure 32

Tripartite logarithmic plot of spectra
for earthquake D-2